5-2011

Operator Splitting Method and Applications for Semilinear Parabolic Partial Differential Equations

R. Corban Harwood
George Fox University, rharwood@georgefox.edu

OPERATOR SPLITTING METHOD AND APPLICATIONS FOR SEMILINEAR PARABOLIC PARTIAL DIFFERENTIAL EQUATIONS

By

RICHARD CORBAN HARWOOD

A dissertation submitted in partial fulfillment of the
requirements for the degree of

DOCTOR OF PHILOSOPHY

WASHINGTON STATE UNIVERSITY
Department of Mathematics

MAY 2011

To the Faculty of Washington State University:

The members of the Committee appointed to examine the dissertation of RICHARD CORBAN HARWOOD find it satisfactory and recommend that it be accepted.

V. S. Manoranjan, Ph.D., Chair

Dean Edwards, Ph.D.

Sergey Lapin, Ph.D.

ACKNOWLEDGEMENT

I am deeply indebted to those who have helped make this dissertation a reality. For training me in mathematical modeling and introducing me to numerical methods, I am forever grateful to my advisor, collaborator, and committee chair, Dr. V. S. "Mano" Manoranjan. Mano guided me in grasping the big picture of the problem at hand, abstracting it to mathematical formulas, analyzing and solving this system using various tools, and then relating my solution back to the real world. I am specifically thankful for this holistic and interdisciplinary perspective which he imprinted upon me. I enjoyed learning many specific nuances and tricks from this master of numerical analysis.

As supervisor and collaborator, Dr. Dean Edwards provided me with invaluable interdisciplinary experience and insight into modeling batteries. Through Dean, I learned to adapt as a mathematician out of my element and work as a team member. It was exciting to see my mathematical methods at work in the real world. For the cooperation and technical expertise in the chemical, material, and structural dynamics of batteries, I would also like to thank my other collaborators at the Center for Intelligent Systems Research, especially Tom Bean, Song Zhang, and John Canning.

Through the myriad of courses I took at Washington State University, I gleaned valuable insight and assistance from numerous professors. For introducing me to operator splitting methods, I am deeply grateful to my committee member, Dr. Sergey Lapin. Sergey helped me experience a variety of problems and methods with which to solve them. Dr. David Wollkind broadened my appreciation for applied mathematics. The grueling asymptotic analysis I completed in his classes prepared me to deal with the nested Taylor expansions necessary in developing and analyzing the numerical methods

used throughout this dissertation. Dr. Alan Genz showed me how to numerically verify a method's accuracy. Dr. Bob Mifflin assisted my development of nonlinear optimization schemes to solve for internal and data-defined model parameters. Dr. Rich Alldredge taught me how to honestly analyze data variance in designed experiments involving battery charge-discharge cycles.

Along with the technical assistance described above, I received equally important assistance from family and friends. My father, Bill, and mother, Ramona, raised me to work hard for my dreams. Their love of music instilled within me a passion for the beautiful simplicity of the song which is only attained by working past the complexity of the notes on the page. This simplicity emerging from complexity is a key theme of my dissertation and my love for mathematics. Together with my sister, two brothers, and extended family, they continue to support me in all my endeavors. My girlfriend, Mary, has also stood with me during this physically and emotionally draining year and I am deeply grateful for her support and assistance.

For the guidance through my undergraduate education as well as the encouragement to continue into graduate research, I personally thank my mathematics advisor at Whitworth University, Dr. Donna Pierce. Donna continues to support me as a mathematician and I appreciate her timely career advice. Also, I would never have gotten through graduate school without the support and camaraderie of my mathematical siblings Andrei Kouznetsov, Bonni Kealy, Matt Labrum, and Li Zhu, as well as my officemates and other fellow graduate students at Washington State University. Their guidance and friendship helped me tremendously throughout this work. Additionally, I would like to thank the administrative and technical staff of the mathematics department for their unfailing service and invaluable help in completing my degree.

OPERATOR SPLITTING METHOD AND APPLICATIONS FOR SEMILINEAR PARABOLIC PARTIAL DIFFERENTIAL EQUATIONS

Abstract

by Richard Corban Harwood, Ph.D.
Washington State University
MAY 2011

Chair: V. S. Manoranjan

This dissertation presents a redefined operator splitting method used in solving semilinear parabolic partial differential equations. As one such form, the reaction-diffusion equation is highly prevalent in mathematical modeling. Besides being physically meaningful as a separation of two distinct physical processes in this equation, operator splitting simplifies the solution method in several ways. The super-linear speed-up of computations is a rewarding simplification as it presents great benefits for large-scale systems. In solving these semilinear equations, we will develop a condition for oscillation-free methods, a condition independent of the usual stability condition. This numerical consideration is important to fully embody our concerns for a method's stability and consistency, and is critical in extending our methods from linear to semilinear problems. The mathematical modeling process will be discussed and demonstrated by developing models from first principles and then reducing them down through simplifying assumptions. These models will be extended to simulate experimental data, using the comparison to real data as validation of the model. Finally, in the face of high data variability, this model validation process will present the need for calibration and further model refinement.

Contents

List of Figures

Chapter 1

INTRODUCTION AND NUMERICAL CONSIDERATIONS

The main components of this dissertation were motivated by a desire for simplicity. Complex problems accompany any study of the real world. To mathematically model physical, chemical, and biological processes, we apply reasonable and useful simplifications at each stage of model development, approximation, and solution. These simplifications are necessary due to our finite knowledge of the universe and useful due to our need for answers in meaningfully short amounts of time.

Our focus on semilinear parabolic partial differential equations is epitomized by the reaction-diffusion equation, which represents two distinct, but simultaneously occurring processes. This distinction between processes, represented by distinct reaction and diffusion operators, originally motivated the use of operator splitting techniques. Besides being physically meaningful, operator splitting simplifies the solution method in several ways. The superlinear speed-up in computations is a rewarding simplification as it presents great benefits for large-scale systems. Numerical considerations like oscillatory behavior and boundary approximations are important to fully embody our concerns for a method's stability and consistency.

1.1 Operator Splitting

Complicated models in environmental science, meteorology, and fluids have given rise to various operator splitting techniques. The goal has always been to simplify: to increase efficiency and computational speed by solving simpler equations which usually represent distinct physical processes [17]. Also known as split-step methods, decoupled operator splitting methods are well known in solving the nonlinear Schrödinger (NLS) equation [20, 36], which has wide physical applications, like Bose-Einstein condensation

and light pulse propagation in optical fibers [10, 39]. Particularly, after splitting the NLS equation into linear and nonlinear parts, the linear part may be solved analytically in frequency domain. Accordingly, this method is also called the split-step Fourier method [43]. Recently, this method has been applied to solve the generalized NLS equations, like Gross-Pitaevskii equation [27], Klein-Gordon equation [24], and so on. Operator splitting breaks a semilinear problem, such as

$$\frac{\partial u}{\partial t} = A(u) + B(u),$$

into a linear diffusion equation and the nonlinear reaction equation.

Operator splitting comes in various forms. Sometimes the domain can be decomposed to facilitate separate physical processes, or at least to isolate the more interesting regions of the domain, as is done with adaptive meshing. At other times, a number of physical processes compete at different rates and decoupling merely severs their weak dependency for the gain of simplicity and efficiency. Or, as in the case we are interested in, the operators are split for algebraic reasons [17].

In this latter type of operator splitting, the simpler equations are solved and then recoupled over the initial conditions in delicate ways to preserve a certain accuracy. Although this type of splitting is tantalizing for nonlinear problems, the methodology is plagued with problems of certain forms and a general analysis of nonlinear splitting is sorely lacking. We seek to not only propose one more example implementation, but to propose and demonstrate some general analysis of splitting methods.

There are many major benefits of operator splitting, including dimension reduction, problem simplification, preservation of any order accuracy in time, and computational speed-up for some complex problems. The reduction in the dimensionality can take

the form of splitting a high dimensional problem into a combination of one-dimensional problems, severely reducing the size of the matrices used in numerical solutions, as exemplified by the Alternate Direction Implicit (ADI) method [26], or it can isolate the spatial dimensionality to one subproblem and remove it from the other, as shown in the battery simulation in section 3. The problem can be simplified, not only in the numerical solutions of all subproblems, but it can also allow for exact solutions of some of the subproblems. Further, these recombinations provide the same order of splitting accuracy for the linear and nonlinear parabolic PDEs. Still, the cost of recombining split solutions must be balanced with the degree of accuracy desired and the computational time allowed. Due to this simplification of problems of certain complexity, operator splitting can immensely increase the efficiency of the solution and provide high levels of speed-up which begs for use in the solution of large systems. As an example in section 3, the first order splitting of a semilinear PDE solved over a one-dimensional composite domain provides superlinear speed-up as the mesh is refined.

Early work in this area of numerical analysis was set forth by Gilbert Strang in the late 1960's [35], before the term "operator splitting" was coined. He developed his "difference scheme" as a recombination of a Lax-Wendroff scheme published few years prior. He provided details of accuracy calculations for his numerical approximation and splitting, and argues for stability in correlation to linear and nonlinear cases [35].

We investigate the credibility and feasibility of nontrivially decoupling a semilinear operator so as to provide computational speed while maintaining accuracy and stability of the numerical solution. We specifically apply this operator splitting to decouple a semilinear operator into separate linear and nonlinear operators which are directly

solvable or computationally cheap to invert. To motivate our investigation of semilinear parabolic PDEs, we begin first with a linear nonhomogeneous ordinary differential equation and then a linear parabolic PDE.

1.1.1 Linear Demonstration

To motivate the development and analysis of this decoupled operator splitting method, we begin with a model problem. Since the application of spatial discretizations to a general parabolic PDE reduces it to an ordinary differential equation (ODE) in terms of time, we begin our investigation of semilinear parabolic PDEs with a simple form of an ODE,

$$\frac{dy}{dt} = y + 1, \; y(0) = 1. \tag{1.1}$$

We will consider a first order splitting of this ODE into split equation 'A',

$$\frac{1}{2}\frac{dy}{dt} = y,$$

and the split equation 'B',

$$\frac{1}{2}\frac{dy}{dt} = 1,$$

and recombine their solutions in a sequential scheme designed to preserve a certain level of accuracy in time. For example, the direct 'AB' recombination scheme results in the piecewise solution,

$$y_{AB}(t) = \begin{cases} e^{2t}, & 0 \leq t \leq \frac{t_f}{2} \\ 2\left(t - \frac{t_f}{2}\right) + e^{t_f}, & \frac{t_f}{2} \leq t \leq t_f \end{cases} \tag{1.2}$$

while reordering the split equations to the 'BA' recombination scheme results in

$$y_{BA}(t) = \begin{cases} 1 + 2t, & 0 \leq t \leq \frac{t_f}{2} \\ (1 + t_f)\, e^{2\left(t - \frac{t_f}{2}\right)}, & \frac{t_f}{2} \leq t \leq t_f. \end{cases} \tag{1.3}$$

Though not differentiable, notice that both piecewise functions (1.2) and (1.3) are continuous. Though the two recombination schemes (1.2) and (1.3) are obviously different, they both preserve a first order approximation in time to the exact solution (1.1), as proven in section 1.1.4 and shown in section 1.1.1.2. Usually, one recombination ordering will overapproximate the exact solution while the other underapproximates it. This is shown in figure 1.

1.1.1.1 Comparison of Full and Split Solutions

The full PDE (1.1) can be solved as a separable differential equation as follows,

$$\begin{aligned} \frac{dy}{dt} &= y + 1, \\ \frac{dy}{y+1} &= dt \\ \ln\left(\frac{y(t)+1}{y(0)+1}\right) &= t \\ y(t) &= (y(0)+1)e^t - 1. \end{aligned}$$

Plugging in our initial condition $y(0) = 1$, we obtain the exact solution to the full equation,

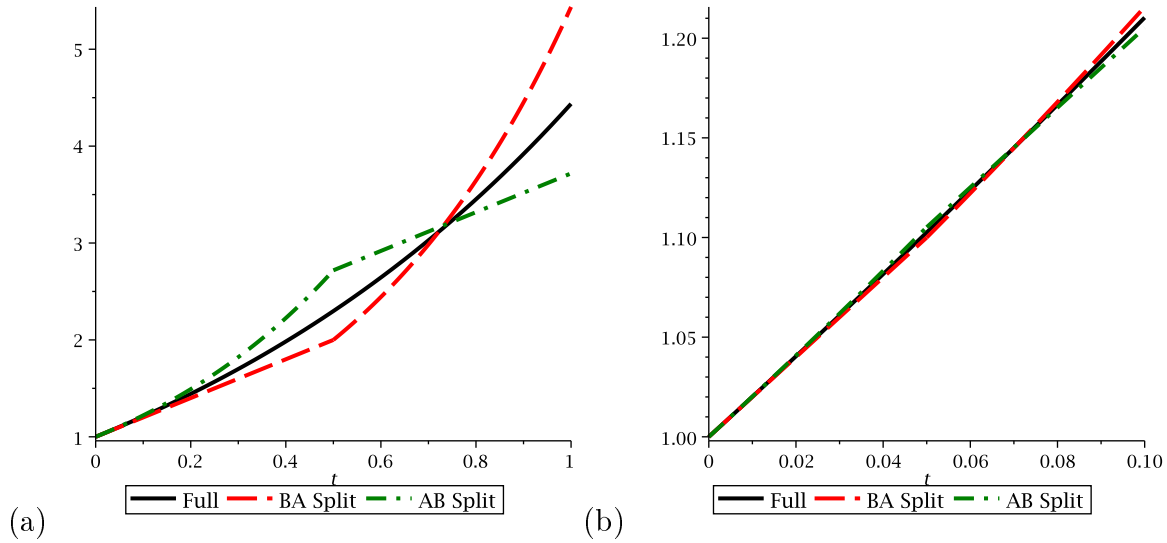

(a) (b)

Figure 1: Comparison between the 'BA' and 'AB' splitting recombinations and the exact full solution for time steps (a) $t_f = 1$ and (b) $t_f = 0.1$.

$$y_F(t) = 2e^t - 1.$$

Figure 1 shows the comparison between the 'AB' and 'BA' split approximations to the full equation for a large and small time step.

1.1.1.2 Accuracy

To demonstrate the splitting method's accuracy, we solve our solution over many small steps, $t_f = \Delta t$, and seek the level at which our error converges to 0 as the time step,Δt, converges to 0. The accuracy of the error due to splitting alone is determined by the order, under Taylor expansion, to which the solutions agree. The first order accuracy in time for the 'AB' recombination is shown through the following Taylor expansions,

$$
\begin{aligned}
|y_F(\Delta t) - y_{AB}(\Delta t)| &= \left|(2e^{\Delta t} - 1) - \left(\Delta t + e^{\Delta t}\right)\right| \\
&= \left|(2\left(1 + \Delta t + \frac{1}{2}\Delta t^2 + O\left(\Delta t^3\right)\right) - 1) \right. \\
&\quad \left. - \left(\Delta t + 1 + \Delta t + \frac{1}{2}\Delta t^2 + O\left(\Delta t^3\right)\right)\right| \\
&= \left|\left(1 + 2\Delta t + \Delta t^2 + O\left(\Delta t^3\right)\right) - \left(1 + 2\Delta t + \frac{1}{2}\Delta t^2 + O\left(\Delta t^3\right)\right)\right| \\
&= \left|\frac{1}{2}\Delta t^2 + O\left(\Delta t^3\right)\right| \\
&= O\left(\Delta t^2\right).
\end{aligned}
$$

Since the error between the full and 'AB'-split solutions is $O\left(\Delta t^2\right)$, the solutions agree up to order $O(\Delta t)$, which is thus the splitting accuracy of the 'AB' recombination scheme. The first order splitting accuracy in time of the 'BA' recombination scheme is similarly shown as

$$
\begin{aligned}
|y_F(\Delta t) - y_{BA}(\Delta t)| &= \left|(2e^{\Delta t} - 1) - (1 + \Delta t)\, e^{\Delta t}\right| \\
&= \left|\left(2\left(1 + \Delta t + \frac{1}{2}\Delta t^2 + O(\Delta t^3)\right) - 1\right) \right. \\
&\quad \left. - (1 + \Delta t)\left(1 + \Delta t + \frac{1}{2}\Delta t^2 + O(\Delta t^3)\right)\right| \\
&= \left|\left(1 + 2\Delta t + \Delta t^2 + O\left(\Delta t^3\right)\right) - \left(1 + 2\Delta t + \frac{3}{2}\Delta t^2 + \frac{2}{3}\Delta t^3 + O(\Delta t^4)\right)\right| \\
&= \left|-\frac{1}{2}\Delta t^2 + O(\Delta t^3)\right| \\
&= O\left(\Delta t^2\right).
\end{aligned}
$$

It is clear now that the splitting error for the two orderings of the first order recombination scheme is not the same but it is of the same order. To produce a higher order

splitting approximation to the ODE, The governing equation would be split as,

$$\frac{1}{4}\frac{dy}{dt} + \frac{1}{4}\frac{dy}{dt} + \frac{1}{4}\frac{dy}{dt} + \frac{1}{4}\frac{dy}{dt} = \frac{1}{2}y + \frac{1}{2}y + \frac{1}{2} + \frac{1}{2}.$$

If we order these quarters as a combination of the two first order recombination orderings, all within in one time step Δt as presented in section 1.1, this would lead to second order splittings which allow us to combine the two inner operations into one, which reduces the number of computations. One of these is the 'ABA' recombination,

$$\frac{1}{4}\frac{dy}{dt} = \frac{1}{2}y, \qquad \frac{1}{2}\frac{dy}{dt} = 1, \qquad \frac{1}{4}\frac{dy}{dt} = \frac{1}{2}y,$$

where the inner two quarter solutions are combined together. The piecewise solution to this recombination is

$$y_{ABA}(t) = \begin{cases} e^{2t}, & 0 \le t \le \frac{t_f}{4} \\ 2\left(t - \frac{t_f}{4}\right) + e^{\frac{t_f}{2}}, & \frac{t_f}{4} \le t \le \frac{3t_f}{4} \\ \left(\frac{t_f}{2} + e^{\frac{t_f}{2}}\right) e^{2\left(t - \frac{t_f}{2}\right)}, & \frac{3t_f}{4} \le t \le t_f. \end{cases}$$

The other is the 'BAB' recombination,

$$y_{BAB}(t) = \begin{cases} 1 + 2t, & 0 \le t \le \frac{t_f}{4} \\ \left(1 + \frac{t_f}{2}\right) e^{2\left(t - \frac{t_f}{4}\right)}, & \frac{t_f}{4} \le t \le \frac{3t_f}{4} \\ \left(1 + \frac{t_f}{2}\right) e^{t_f} + 2\left(t - \frac{3t_f}{4}\right), & \frac{3t_f}{4} \le t \le t_f. \end{cases}$$

Figure 2 shows the comparison between the 'ABA' and 'BAB' split approximations to the full equation for large and small time steps.

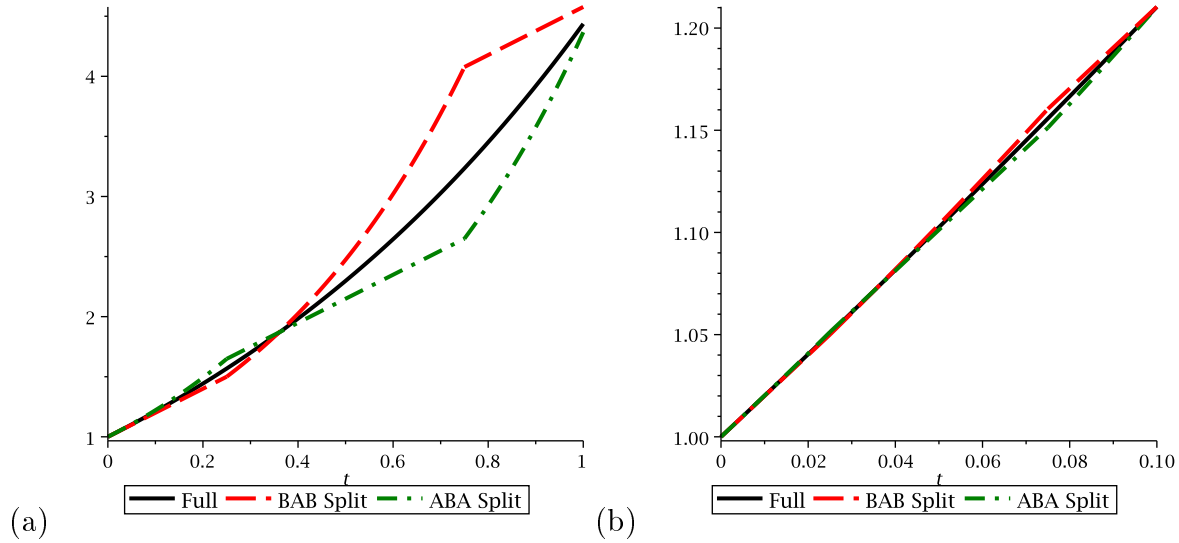

(a) (b)

Figure 2: Comparison between two second order splitting recombinations, 'BAB' and 'ABA', and the exact full solution for time steps (a) $t_f = 1$ and (b) $t_f = 0.1$.

1.1.2 Linear Theory

To introduce the method, we write our semilinear parabolic PDE in operator form as a general reaction-diffusion equation,

$$\frac{\partial u(x,t)}{\partial t} = D(u(x,t)) + R(u(x,t)), \tag{1.4}$$

where D and R are spatial discretizations (matrices) of linear or linearized operators, assuming a local linearization of the problem. The exact solution of equation (1.4) is then approximated by

$$u^{n+1} = e^{\Delta t(D+R)}u^n,$$

where $u^n = u(x, n\Delta t)$ with Δt being the time step.

We then separate the two linearized operators into the split equations,

$$\frac{1}{2}\frac{\partial u}{\partial t} = Du, \tag{1.5}$$

$$\frac{1}{2}\frac{\partial u}{\partial t} = Ru, \tag{1.6}$$

which are then solved sequentially over the set of subintervals $\left\{\left[t_n, t_n + \frac{\Delta t}{2}\right], \left[t_n + \frac{\Delta t}{2}, t_{n+1}\right]\right\}$, where $t_{n+1} = t_n + \Delta t$. By separating the diffusion and reaction terms as in (1.5) and (1.6), where an intermediate solution is obtained at $t = t_n + \frac{\Delta t}{2}$ by solving the reaction equation (1.6), and then using it as the initial solution to solve the diffusion equation (1.5) for another half step to obtain the solution at $t = \Delta t$. Consequently, we may write the solution for one global time step as,

$$u^{n+1} = e^{\Delta t D} e^{\Delta t R} u^n. \tag{1.7}$$

Or we may switch the solving order such that the solution over the same time step is

$$u^{n+1} = e^{\Delta t R} e^{\Delta t D} u^n. \tag{1.8}$$

One advantage of this splitting is that it reduces the semilinear problem to the well known diffusion problem which could be solved with a suitable numerical scheme. Another advantage is that an exact solution might be found for the non-linear reaction term using standard differential equation methods (as shown in section 2.2 for Fisher-type equation), so that a portion of the error generated from common numerical methods could be eliminated. During the split, however, an extra error has been introduced. In a later section, we will prove this splitting error to be first order in time for general semilinear parabolic PDEs.

To obtain a second-order time accuracy for split-step method, we need to maintain the symmetry of the solution. One straight-forward method is taking an average of the two solutions (1.7) and (1.8),

$$u^{n+1} = \frac{e^{\Delta t R} e^{\Delta t D}}{2} u^n + \frac{e^{\Delta t D} e^{\Delta t R}}{2} u^n, \tag{1.9}$$

however, this requires us to numerically solve the diffusion portion twice in equation (1.9). Since the reaction part is solved exactly, the computational cost of the method is roughly twice the cost of a numerical matrix inversion every time step. Looking at the splitting in a slightly different way allows us to cut our computations in half.

1.1.3 Accuracy of Split Recombination Schemes

Accuracy analysis, as with stability analysis, is based upon linear theory. Thus, to understand and motivate the accuracy computations in recombining the split operators, we will consider the splitting error for the given linear problem and then generalize.

Again, suppose that our problem originates with linearized and spatially discretized operators, D and R. Assuming we can invert the operators exactly, at each time interval we can calculate the exact solution of the full differerential equation

$$\frac{\partial u}{\partial t} = (D + R)u,$$

as

$$u^{n+1} = e^{\Delta t(D+R)}u^n.$$

Splitting this equation into the set of split equations,

$$\left\{\frac{1}{2}\frac{\partial u}{\partial t} = Ru,\ \frac{1}{2}\frac{\partial u}{\partial t} = Du\right\},$$

which are solved over the subintervals

$$\left\{\left[t_n, t_n + \frac{\Delta t}{2}\right], \left[t_n + \frac{\Delta t}{2}, t_{n+1}\right]\right\},$$

the split solution is

$$u^{n+1} = e^{\Delta t D} e^{\Delta t R} u^n.$$

Thus, the splitting accuracy is found by comparing these solutions under Taylor expansion. By exponentiation, the matrix operations on u^n are

$$\begin{aligned}
e^{\Delta t(D+R)} &= \sum_{k=0}^{\infty} \frac{\Delta t^k (D+R)^k}{k!} \\
&= I + \Delta t(D+R) + \frac{\Delta t^2}{2}(D+R)^2 + \frac{\Delta t^3}{6}(D+R)^3 + O\left(\Delta t^4\right) \\
e^{\Delta t D} e^{\Delta t R} &= \left[\sum_{k=0}^{\infty} \frac{\Delta t^k D^k}{k!}\right]\left[\sum_{k=0}^{\infty} \frac{\Delta t^k R^k}{k!}\right] \\
&= \left[I + \Delta t D + \frac{\Delta t^2}{2} D^2 + O\left(\Delta t^3\right)\right]\left[I + \Delta t R + \frac{\Delta t^2}{2} R^2 + O\left(\Delta t^3\right)\right] \\
&= I + \Delta t(D+R) + \frac{\Delta t^2}{2}(D^2 + 2DR + R^2) + O\left(\Delta t^3\right).
\end{aligned}$$

Computing the difference of these two solutions to be $O\left(\Delta t^2\right)$,

$$\begin{aligned}
\left[e^{\Delta t(D+R)} - e^{\Delta t D} e^{\Delta t R}\right] u^n &= \left[\Delta t^2 \frac{(RD - DR)}{2} + O\left(\Delta t^3\right)\right] u^n \\
&= O\left(\Delta t^2\right),
\end{aligned}$$

we obtain the first order splitting accuracy. Recall that the order of truncation in splitting the operators corresponds to order of agreement in solution.

Further, if matrices D and R commute, then there is no error due to the splitting. Matrices only commute with diagonal matrices and other matrices in their similarity class, particularly themselves [40]. Since we do not consider any trivial operator splitting (that is, $A = A + 0$), commutating matrices are a rare occurrence.

Let us now consider a splitting scheme that alternates the order of split solution multiple times within one global step. This type of operator splitting was originally

proposed as a second order symmetric method by Strang [35]. Specifically for a second order splitting scheme, we divide the full equation into four components,

$$\frac{1}{4}\frac{\partial u}{\partial t}+\frac{1}{4}\frac{\partial u}{\partial t}+\frac{1}{4}\frac{\partial u}{\partial t}+\frac{1}{4}\frac{\partial u}{\partial t}=\frac{1}{2}Ru+\frac{1}{2}Du+\frac{1}{2}Du+\frac{1}{2}Ru,$$

alternating the operator order. Solving these four split equations sequentially, and combining the inner two split equations without error because D commutes with itself, we essentially solve the set of split equations,

$$\left\{\frac{\partial u}{\partial t}=2Ru,\frac{\partial u}{\partial t}=2Du,\frac{\partial u}{\partial t}=2Ru\right\},$$

over the subintervals,

$$\left\{\left[t_n,t_n+\frac{\Delta t}{4}\right],\left[t_n+\frac{\Delta t}{4},t_n+\frac{3\Delta t}{4}\right],\left[t_n+\frac{3\Delta t}{4},t_{n+1}\right]\right\},$$

to obtain the split solution over each global interval,

$$u^{n+1}=e^{\frac{\Delta t}{2}R}e^{\Delta tD}e^{\frac{\Delta t}{2}R}u^n.$$

Then, computing the difference between the full and split solutions, we obtain solution agreement up to $O\left(\Delta t^2\right)$,

$$\left[e^{\Delta t(D+R)}-e^{\frac{\Delta t}{2}R}e^{\Delta tD}e^{\frac{\Delta t}{2}R}\right]u^n \;=\; O(\Delta t^3),$$

making this alternating splitting method second order accurate in time. Note that this accuracy is only for the operator splitting itself. To compute the accuracy of the entire splitting method, we would need to include the spatial discretization error as well as the solution error for the actual method used to solve each split equation. Matrix

exponentian, though without error theoretically, is computationally intensive as an approximation of an infinite series.

Since this analysis only applies when $D(u)$ and $R(u)$ are linear operators, we cannot rely on matrix exponentiation, even theoretically, for nonlinear split equations and thus turn to direct Taylor expansions about the solution at each subinterval step.

1.1.4 Proof of Semilinear Operator Splitting Accuracy

Sequential combination of split solutions from a decoupled operator splitting method applied to a semilinear parabolic partial differential equation results in the same splitting error as for linear differential equations. Proof of this is shown for first and second order split recombinations

Theorem 1.1. Local Neighborhood Splitting

Given an autonomous, semilinear parabolic PDE, which can be nontrivially written as $\frac{\partial u}{\partial t} = \mathcal{L}u + \mathcal{N}(u)$, *where* $\mathcal{L}$ *and* $\mathcal{N}$ *are linear and nonlinear operators upon* u, *respectively, the solutions to the set of split equations,*

$$\left\{ \frac{1}{2}\frac{\partial u}{\partial t} = \mathcal{N}(u), \frac{1}{2}\frac{\partial u}{\partial t} = \mathcal{L}u \right\},$$

provide an $O(\Delta t)$ *splitting accuracy when solved sequentially over the set of subintervals,*

$$\left\{ \left[t_n, t_n + \frac{\Delta t}{2} \right], \left[t_n + \frac{\Delta t}{2}, t_{n+1} \right] \right\},$$

and further, that reversing the order of the split equations to

$$\left\{\frac{1}{2}\frac{\partial u}{\partial t} = \mathcal{L}u, \frac{1}{2}\frac{\partial u}{\partial t} = \mathcal{N}(u)\right\},$$

provides the same $O(\Delta t)$ splitting accuracy when solved sequentially over the same set of subintervals.

Proof. Suppose we have a semilinear parabolic partial differential equation which can be separated into linear and nonlinear components 1.4, and has been discretized in space to the form,

$$\frac{\partial u^n}{\partial t} = Lu^n + N\left(u^n\right),$$

where L is an $m \times m$ matrix discretization of operator$\mathcal{L}$ and $N\left(u^n\right)$ is an $m-$dimensional vector discretization of operator $\mathcal{N}(u)$.

Using Taylor expansions at time step $t_{n+1} = t_n + \Delta t$, the solution to the full problem, $u_F^{n+1} = u_F\left(t_{n+1}\right)$, is

$$\begin{aligned}
u_F^{n+1} &= u^n + \Delta t\frac{\partial u^n}{\partial t} + \frac{\Delta t^2}{2}\frac{\partial^2 u^n}{\partial t^2} + O(\Delta t^3) \\
&= u^n + \Delta t\left(Lu^n + N\left(u^n\right)\right) + \frac{\Delta t^2}{2}\frac{\partial Lu^n + N(u^n)}{\partial t} + O(\Delta t^3) \\
&= u^n + \Delta t\left(Lu^n + N\left(u^n\right)\right) + \frac{\Delta t^2}{2}\left(L\frac{\partial u^n}{\partial t} + \frac{\partial N}{\partial u^n}\frac{\partial u^n}{\partial t}\right) + O(\Delta t^3) \\
&= u^n + \Delta t\left(Lu^n + N\left(u^n\right)\right) \\
&\quad + \frac{\Delta t^2}{2}\left(L^2u^n + LN\left(u^n\right) + \frac{\partial N(u^n)}{\partial u^n}Lu^n\frac{\partial N(u^n)}{\partial u^n}N\left(u^n\right)\right) + O(\Delta t^3).
\end{aligned}$$

The 'NL' recombination of the split solutions gives the following approximation by

Taylor expansions

$$
\begin{aligned}
u_{NL}^{n+1} &= e^{\Delta t L} u^{n+1/2} \\
&= \left(I + \Delta t L + \frac{\Delta t^2}{2} + O(\Delta t^3) \right) \left(u^n + \frac{\Delta t}{2} \frac{\partial u^n}{\partial t} + \frac{\Delta t^2}{8} \frac{\partial^2 u^n}{\partial t^2} + O(\Delta t^3) \right) \\
&= \left(I + \Delta t L + \frac{\Delta t^2}{2} + O(\Delta t^3) \right) \left(u^n + \Delta t N(u^n) + \frac{\Delta t^2}{2} \frac{\partial N(u^n)}{\partial t} + O(\Delta t^3) \right) \\
&= u^n + \Delta t \left(L u^n + N(u^n) \right) + \frac{\Delta t^2}{2} \left(L^2 u^n + 2LN(u^n) + \frac{\partial N(u^n)}{\partial u^n} N(u^n) \right) + O(\Delta t^3),
\end{aligned}
$$

where $\frac{\partial u^{n+1/2}}{\partial t} = 2N(u^{n+1/2})$. The $O\left(\Delta t\right)$ splitting error can be obtained by computing the $O\left(\Delta t^2\right)$ solution difference for this ordering as

$$
\begin{aligned}
\left| u_F^{n+1} - u_{NL}^{n+1} \right| = & \left| \left[u^n + \Delta t \left(L u^n + N\left(u^n\right) \right) \right. \right. \\
& \left. + \frac{\Delta t^2}{2} \left(L^2 u^n + LN\left(u^n\right) + \frac{\partial N(u^n)}{\partial u^n} L u^n + \frac{\partial N\left(u^n\right)}{\partial u^n} N\left(u^n\right) \right) + O\left(\Delta t^3\right) \right] \\
& - \left[u^n + \Delta t \left(L u^n + N\left(u^n\right) \right) \right. \\
& \left. \left. + \frac{\Delta t^2}{2} \left(L^2 u^n + 2LN\left(u^n\right) + \frac{\partial N\left(u^n\right)}{\partial u^n} N\left(u^n\right) \right) + O\left(\Delta t^3\right) \right] \right| \\
= & \left| \frac{\Delta t^2}{2} \left(\frac{\partial N(u^n)}{\partial u^n} L u^n - LN\left(u^n\right) \right) + O\left(\Delta t^3\right) \right| \\
= & O\left(\Delta t^2\right).
\end{aligned}
$$

The 'LN' recombination gives

$$
\begin{aligned}
u_{LN}^{n+1} =& u^{n+1/2} + \frac{\Delta t}{2}\frac{\partial u^{n+1/2}}{\partial t} + \frac{\Delta t^2}{8}\frac{\partial^2 u^{n+1/2}}{\partial t^2} + O\left(\Delta t^3\right) \\
=& u^{n+1/2} + \Delta t N(u^{n+1/2}) + \frac{\Delta t^2}{2}\frac{\partial N\left(u^{n+1/2}\right)}{\partial t} + O\left(\Delta t^3\right) \\
=& e^{\Delta t L}u^n + \Delta t N(e^{\Delta t L}u^n) + \frac{\Delta t^2}{2}\frac{\partial N\left(e^{\Delta t L}u^n\right)}{\partial t} + O\left(\Delta t^3\right) \\
=& \left(I + \Delta t L + \frac{\Delta t^2}{2}L^2 + O\left(\Delta t^3\right)\right)u^n + \Delta t N\left(u^n + \Delta t L u^n + O\left(\Delta t^2\right)\right) \\
=& + \frac{\Delta t^2}{2}\frac{\partial N\left(u^n + O\left(\Delta t\right)\right)}{\partial t} + O\left(\Delta t^3\right) \\
=& u^n + \Delta t L u^n + \frac{\Delta t^2}{2}L^2 u^n + \Delta t\left(N(u^n) + \Delta t\frac{dN}{du^n}Lu^n + O(\Delta t^2)\right) \\
&+ \frac{\Delta t^2}{2}\frac{\partial N\left(u^n\right)}{\partial t} + O\left(\Delta t^3\right) \\
=& u^n + \Delta t\left(Lu^n + N(u^n)\right) + \frac{\Delta t^2}{2}\left(L^2 u^n + 2\frac{dN}{du^n}Lu^n + \frac{\partial N(u^n)}{\partial u^n}N(u^n)\right) + O(\Delta t^3),
\end{aligned}
$$

where $u^{n+1/2} = e^{\Delta t L}u^n$ solves $\frac{\partial u^{n+1/2}}{\partial t} = 2N\left(u^{n+1/2}\right)$. The $O\left(\Delta t\right)$ splitting error can be obtained by computing the $O\left(\Delta t^2\right)$ solution difference for this ordering as

$$
\begin{aligned}
\left|u_F^{n+1} - u_{LN}^{n+1}\right| =& \Big|\Big[u^n + \Delta t\left(Lu^n + N\left(u^n\right)\right) \\
&+ \frac{\Delta t^2}{2}\left(L^2 u^n + LN\left(u^n\right) + \frac{\partial N(u^n)}{\partial u^n}Lu^n + \frac{\partial N\left(u^n\right)}{\partial u^n}N\left(u^n\right)\right) + O\left(\Delta t^3\right)\Big] \\
&- \Big[u^n + \Delta t\left(Lu^n + N\left(u^n\right)\right) \\
&+ \frac{\Delta t^2}{2}\left(L^2 u^n + 2\frac{\partial N\left(u^n\right)}{\partial u^n}Lu^n + \frac{\partial N\left(u^n\right)}{\partial u^n}N\left(u^n\right)\right) + O\left(\Delta t^3\right)\Big]\Big| \\
=& \left|\frac{\Delta t^2}{2}\left(LN\left(u^n\right) - \frac{\partial N(u^n)}{\partial u^n}Lu^n\right) + O\left(\Delta t^3\right)\right| \\
=& O\left(\Delta t^2\right).
\end{aligned}
$$

Hence, the computations for both split orderings of the parabolic equation gives first order accuracy in time. □

Our next theorem makes use of the fact that matrices commute with themselves to decrease the number of computations needed for a second order split recombination. In this case, the number of times the diffusion split equation is solved is reduced.

Theorem 1.2. Second Order Symmetric Splitting

Given an autonomous, semilinear parabolic PDE, which can be nontrivially written as $\frac{\partial u}{\partial t} = \mathcal{L}u + \mathcal{N}(u)$*, where* $\mathcal{L}$ *and* $\mathcal{N}$ *are linear and nonlinear operators upon* u*, respectively, the solutions to the set of split equations,*

$$\left\{ \frac{1}{4}\frac{\partial u}{\partial t} = \frac{\mathcal{N}(u)}{2}, \frac{1}{2}\frac{\partial u}{\partial t} = \mathcal{L}u, \frac{1}{4}\frac{\partial u}{\partial t} = \frac{\mathcal{N}(u)}{2} \right\},$$

provide an $O\left(\Delta t^2\right)$ *splitting accuracy when solved sequentially over the set of subintervals,*

$$\left\{ \left[t_n, t_n + \frac{\Delta t}{4} \right], \left[t_n + \frac{\Delta t}{4}, t_n + \frac{3\Delta t}{4} \right], \left[t_n + \frac{3\Delta t}{4}, t_{n+1} \right] \right\}.$$

Proof. Suppose we have a semilinear parabolic partial differential equation which can be separated into linear and nonlinear components (1.4), and has been discretized in space to the form,

$$\frac{\partial u^n}{\partial t} = Lu^n + N\left(u^n\right),$$

where L is an $m \times m$ matrix discretization of operator $\mathcal{L}$ and $N\left(u^n\right)$ is an $m-$dimensional vector discretization of operator $\mathcal{N}(u)$.

Using Taylor expansions at time step $t_{n+1} = t_n + \Delta t$, the solution to the full problem

is

$$\begin{aligned} u_F^{n+1} =& u^n + \Delta t \left(L u^n + N\left(u^n\right)\right) \\ &+ \frac{\Delta t^2}{2} \left(L^2 u^n + LN\left(u^n\right) + \frac{\partial N(u^n)}{\partial u^n} L u^n \frac{\partial N(u^n)}{\partial u^n} N\left(u^n\right) \right) + O(\Delta t^3). \end{aligned}$$

The given 'NLN' recombination of the split solutions gives the following approximation by Taylor expansions,

$$
\begin{aligned}
u_{NLN}^{n+1} =& u^{n+3/4} + \frac{\Delta t}{4}\frac{\partial u^{n+3/4}}{\partial t} + \frac{\Delta t^2}{32}\frac{\partial^2 u^{n+3/4}}{\partial t^2} + O\left(\Delta t^3\right) \\
=& u^{n+3/4} + \frac{\Delta t}{2} N\left(u^{n+3/4}\right) + \frac{\Delta t^2}{8}\frac{\partial N\left(u^{n+3/4}\right)}{\partial t} + O\left(\Delta t^3\right) \\
=& e^{\Delta t L} u^{n+1/4} + \frac{\Delta t}{2} N\left(e^{\Delta t L} u^{n+1/4}\right) + \frac{\Delta t^2}{8}\frac{\partial N\left(e^{\Delta t L} u^{n+1/4}\right)}{\partial t} + O\left(\Delta t^3\right) \\
=& \left(I + \Delta t L + \frac{\Delta t^2}{2} L^2 + O(\Delta t^3)\right) u^{n+1/4} + \frac{\Delta t}{2} N\left(\left(I + \Delta t L + O\left(\Delta t^2\right)\right) u^{n+1/4}\right) \\
&+ \frac{\Delta t^2}{8}\frac{\partial N\left(u^{n+1/4} + O\left(\Delta t\right)\right)}{\partial t} + O\left(\Delta t^3\right) \\
=& \left(I + \Delta t L + \frac{\Delta t^2}{2} L^2 + O(\Delta t^3)\right) u^{n+1/4} \\
&+ \frac{\Delta t}{2}\left(N\left(u^{n+1/4}\right) + \Delta t \frac{\partial N\left(u^{n+1/4}\right)}{\partial u^{n+1/4}} L u^{n+1/4} + O\left(\Delta t^2\right)\right) \\
&+ \frac{\Delta t^2}{16}\frac{\partial N\left(u^{n+1/4}\right)}{\partial t} + O\left(\Delta t^3\right) \\
=& \left(I + \Delta t L + \frac{\Delta t^2}{2} L^2 + O(\Delta t^3)\right)\left(u^n + \frac{\Delta t}{4}\frac{\partial u^n}{\partial t} + \frac{\Delta t^2}{32}\frac{\partial^2 u^n}{\partial t^2} + O\left(\Delta t^3\right)\right) \\
&+ \frac{\Delta t}{2}\left(N\left(u^n + \frac{\Delta t}{4}\frac{\partial u^n}{\partial t} + O\left(\Delta t^2\right)\right) + \Delta t \frac{\partial N\left(u^n + O\left(\Delta t\right)\right)}{\partial u^n + O(\Delta t)} L\left(u^n + O\left(\Delta t\right)\right)\right) \\
&+ \frac{\Delta t^2}{16}\frac{\partial N\left(u^n + O\left(\Delta t\right)\right)}{\partial t} + O\left(\Delta t^3\right) \\
=& \left(I + \Delta t L + \frac{\Delta t^2}{2} L^2 + O(\Delta t^3)\right)\left(u^n + \frac{\Delta t}{2} N\left(u^n\right) + \frac{\Delta t^2}{16}\frac{\partial N\left(u^n\right)}{\partial t} + O\left(\Delta t^3\right)\right) \\
&+ \frac{\Delta t}{2}\left(N\left(u^n + \frac{\Delta t}{2} N\left(u^n\right) + O\left(\Delta t^2\right)\right) + \Delta t \frac{\partial N\left(u^n\right)}{\partial u^n} L u^n + O\left(\Delta t^2\right)\right) \\
&+ \frac{\Delta t^2}{16}\frac{\partial N\left(u^n\right)}{\partial t} + O\left(\Delta t^3\right) \\
=& u^n + \Delta t\left(L + \frac{1}{2} N\left(u^n\right)\right) + \Delta t^2\left(\frac{1}{2} L^2 + \frac{1}{2} L N\left(u^n\right) + \frac{1}{8}\frac{\partial N\left(u^n\right)}{\partial u^n} N\left(u^n\right)\right) + O\left(\Delta t^3\right) \\
&+ \frac{\Delta t}{2} N\left(u^n\right) + \Delta t^2\left(\frac{1}{4}\frac{\partial N\left(u^n\right)}{\partial u^n} N\left(u^n\right) + \frac{1}{2}\frac{\partial N\left(u^n\right)}{\partial u^n} L u^n\right) \\
&+ \frac{\Delta t^2}{8}\frac{\partial N\left(u^n\right)}{\partial u^n} N\left(u^n\right) + O\left(\Delta t^3\right) \\
=& u^n + \Delta t\left(L u^n + N(u^n)\right) \\
&+ \frac{\Delta t^2}{2}\left(L^2 u^n + L N\left(u^n\right) + \frac{\partial N\left(u^n\right)}{\partial u^n} L u^n + \frac{\partial N\left(u^n\right)}{\partial u^n} N\left(u^n\right)\right) + O\left(\Delta t^3\right),
\end{aligned}
$$

where $u^{n+3/4} = e^{\Delta t L} u^{n+1/4}$ solves $\frac{\partial u^{n+3/4}}{\partial t} = 2N\left(u^{n+3/4}\right)$ and $\frac{\partial u^{n+1/4}}{\partial t} = 2N\left(u^{n+1/4}\right)$. The $O\left(\Delta t^2\right)$ splitting error can be obtained by computing the $O\left(\Delta t^3\right)$ solution difference for this ordering as

$$\begin{aligned}
\left|u_F^{n+1} - u_{NLN}^{n+1}\right| = & \left|\left[u^n + \Delta t\left(Lu^n + N\left(u^n\right)\right)\right.\right. \\
& \left. + \frac{\Delta t^2}{2}\left(L^2 u^n + LN\left(u^n\right) + \frac{\partial N(u^n)}{\partial u^n} L u^n + \frac{\partial N\left(u^n\right)}{\partial u^n} N\left(u^n\right)\right) + O\left(\Delta t^3\right)\right] \\
& - \left[u^n + \Delta t\left(Lu^n + N\left(u^n\right)\right)\right. \\
& \left.\left. + \frac{\Delta t^2}{2}\left(L^2 u^n + LN\left(u^n\right) + \frac{\partial N\left(u^n\right)}{\partial u^n} L u^n + \frac{\partial N\left(u^n\right)}{\partial u^n} N\left(u^n\right)\right) + O\left(\Delta t^3\right)\right]\right| \\
= & O\left(\Delta t^3\right).
\end{aligned}$$

Thus, the symmetric splitting results in second order splitting accuracy in time.

□

1.2 Oscillatory Behavior

Another major consideration for numerical methods is their possible oscillatory behavior. Although stability and consistency are the standard verifications for methods, they do not cover all the bases. As shown in subsection 1.2.1 below, methods with verified linearized stability, that is where the stability of the linearized method is verified, can produce oscillatory behavior which can lead to instabilities in the numerical solution of nonlinear equations. Thus, verifying that a method is oscillation-free, as a further restriction to the stability condition, is important for linear equations and critical for nonlinear equations.

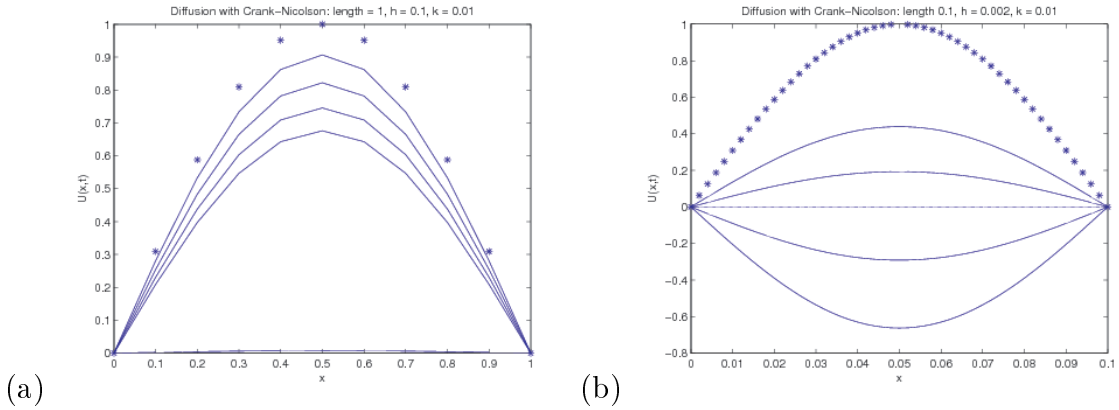

(a) (b)

Figure 3: Conditional oscillatory behavior in heat equation solved by CN method: (a) Unconditionally stable and conditionally oscillation-free, (b) Unconditionally stable and oscillatory.

1.2.1 Inadequacy of Linearized Stability Conditions

The Crank-Nicolson (CN) method [8] is a popular semi-implicit method lauded for its unconditional stability and second order accuracy in both space and time. In solving even a linear diffusion problem, however, it can result in conditional oscillations. This oscillatory behavior is shown in figure 3 for the simple heat equation with Dirichlet boundary conditions (1.12).

1.2.2 Oscillation-Free Conditions

Before we define the oscillation-free and approximate stability conditions we use in later sections, let us recall the stability conditions for spectral and Von Neumann stability analyses. For spectral stability analysis of a linear parabolic PDE [6], a numerical method is stable for the whole solution domain as long as the bound, $|\mu_i| < 1$, applies for all eigenvalues, μ_i, for $i = 1, 2, ..., N$ of the associated $N \times N$ matrix A used in the

time iteration

$$u^{n+1} = Au^n. \tag{1.10}$$

For Von Neumann stability analysis of a linear parabolic PDE [6], a numerical method is stable for the solution away from the domain boundaries as long as the bound, $\left|e^{\gamma \Delta t}\right| < 1$, applies for the error factor in time, $e^{\gamma \Delta t}$, for all inner solutions, $u_{i_*}^{n+1}$, of the associated system

$$\sum_{i=1}^{N} \alpha_i u_i^{n+1} = \sum_{i=1}^{N} \beta_i u_i^n,$$

where i_* is not the index of any boundary node. Combined with the solutions at the boundaries, these equations form the same time iteration matrix (1.10) used in the spectral stability.

Though spectral stability bounds the magnitude of the eigenvalues by one, oscillations can occur when the real part of any of these eigenvalues are negative. Due to sign oscillation as these eigenvalues are powered up, the solution to a linear differential equation oscillates about the final solution. Being stable, these oscillations will dampen out over time, but may move the solution out of the feasibility range, as shown in Figure 3. Oscillatory behavior can actually destabilize solutions to semilinear differential equations. In section 2.2 we impose oscillation-free conditions to show how these instabilities can be controlled for semilinear PDEs.

Definition 1.3. Oscillation-Free

We say that a numerical method for a parabolic PDE is oscillation-free if the real parts, $Re\,(\mu_i)$, of all the eigenvalues of the associated $N \times N$ matrix A_n used in the time iteration $u^{n+1} = A_n u^n$, where the matrix may be updated at each step, are all nonnegative,

$$Re\,(\mu_i) \geq 0,\ i = 1, 2, ..., N,$$

or equivalently when eigenvalues are not attainable, if the Von Neumann error factor for the same matrix A_n is similarly bounded as

$$Re\left(e^{\gamma \Delta t}\right) \geq 0.$$

Note that if a numerical method has all real eigenvalues, or equivalently real error factors, then this method is stable and oscillation-free if $0 < \mu_i < 1$, or $0 < e^{\gamma \Delta t} < 1$, respectively.

Definition 1.4. Approximate Stability

We say that a numerical method for a parabolic PDE is approximately stable if all the eigenvalues of the associated $N \times N$ matrix A_n used in the time iteration $u^{n+1} = A_n u^n$, where the matrix may be updated at each step, are bounded by

$$|\mu_i| < 1 + \Delta t,\ i = 1, 2, ..., N,$$

or equivalently when eigenvalues are not attainable, if the Von Neumann error factor for the same matrix A_n is similarly bounded as

$$\left|e^{\gamma \Delta t}\right| \leq 1 + \Delta t.$$

Assuming that the solution to the parabolic PDE is exponential in nature, this approximate stability bound,

$$\left|e^{\gamma \Delta t}\right| \leq 1 + \Delta t < e^{\Delta t},$$

would keep the error from over taking the solution and thus blowing up.

1.2.3 Special Triadiagonal Matrices

When the eigenvalues of a matrix can be easily calculated, the stability conditions are determined by bounding the magnitude of all eigenvalues. For example, tridiagonal matrices of the form

$$A = \begin{bmatrix} a & c & & 0 \\ b & a & \ddots & \\ & \ddots & \ddots & c \\ 0 & & b & a \end{bmatrix}, \tag{1.11}$$

have eigenvalues specified by

$$\mu^{(i)} = a + 2\sqrt{bc}\cos\left(\frac{i\pi}{N+1}\right),\ i = 1, 2, \ldots, N$$

and eigenvectors, $u^{(i)}$, specified by component k as

$$u_k^{(i)} = \sqrt{\frac{b}{c}}^{k-1} \sin\left(\frac{ik\pi}{N+1}\right),\ i = 1, 2, \ldots, N,\ k = 1, 2, ..., N$$

as long as we assume the first component is $u_1^{(i)} = \sin\left(\frac{i\pi}{N+1}\right),\ i = 1, 2, \ldots, N$ [41].

This matrix form is useful for several numerical methods solving PDEs with Dirichlet boundary conditions, $u|_{\Gamma_l} = \alpha_l$, corresponding to boundary l, notated as Γ_l.

For the explicit Euler method for the heat equation with zero Dirichlet boundary conditions,

$$\begin{aligned} \frac{\partial u}{\partial t} =& \frac{\partial^2 u}{\partial x^2}, \\ u(x,0) =& u_0(x) \\ u(0,t) =& 0, \\ u(L,t) =& 0, \end{aligned} \tag{1.12}$$

the difference equation,

$$u^{n+1} = A_{ED} u^n, \tag{1.13}$$

has the matrix form,

$$A_{ED} = \begin{bmatrix} 1-2\lambda & \lambda & & 0 \\ \lambda & 1-2\lambda & \ddots & \\ & \ddots & \ddots & \lambda \\ 0 & & \lambda & 1-2\lambda \end{bmatrix},$$

for simplifying factor $\lambda = \frac{\Delta t}{\Delta x^2}$. With $a = 1 - 2\lambda$ and $b = c = \lambda$, matrix A_{ED} has eigenvalues

$$\mu^{(i)}(\lambda) = 1 - 4\lambda \sin^2\left(\frac{i\pi}{2\,(N+1)}\right),\ i = 1, 2, \ldots, N \tag{1.14}$$

and corresponding eigenvectors specified by components k as

$$u_k^{(i)} = \sin\left(\frac{ik\pi}{N+1}\right),\ i = 1, 2, \ldots, N,\ k = 1, 2, ..., N.$$

Note that though the eigenvalues depend on λ, their corresponding eigenvectors do not. This means that matrices with different λ values share the same eigenvectors, and will be useful later when proving stability.

Stability of this explicit method requires that $\left|\mu^{(i)}\right| < 1$, that is $\lambda < \frac{1}{2}$. Unfortunately, this stability condition only bounds the eigenvalues between -1 and $+1$; a further restriction of $\lambda < \frac{1}{4}$ bounds the eigenvalues between 0 and 1 and prevents oscillations in the numerical solution. The forward Euler method is a clear example when the oscillation-free condition is a stronger form of the stability condition.

When eigenvalues are not as easily computed, stability of the inner node solution can be determined via Von Neumann analysis (also known as Fourier stability analysis) [6]. This form of stability analysis presupposes that the numerical error at any step can be represented by the exponential form,

$$U_{i+1}^{n+1} - u_{i+1}^{n+1} = e^{\gamma(t_n+\Delta t)} e^{j\beta_m(x_i+\Delta x)},$$

where $U_{i+1}^{n+1}$and u_{i+1}^{n+1} are the exact and approximate solutions to the discretized model (e.g. equation (1.13)), γ is the time constant, $\beta_m = \frac{\pi m}{L}$ are the spatial wavenumbers for $m = 1, 2, \ldots, \frac{L}{\Delta x}$, and $j = \sqrt{-1}$.

Using this exponential form, the error for the previously described forward Euler method with matrix A_{ED} is determined as

$$
\begin{aligned}
u_i^{n+1} =& \lambda u_{i-1}^n + (1-2\lambda)\, u_i^n + \lambda u_{i+1}^n \\
e^{\gamma(t_n+\Delta t)} e^{j\beta x_i} =& \lambda e^{\gamma t_n} e^{j\beta_m (x_i - \Delta x)} + (1-2\lambda)\, e^{\gamma \Delta t} e^{i\beta_m j \Delta x} + \lambda e^{\gamma \Delta t} e^{j\beta_m (x_i + \Delta x)} \\
e^{\gamma \Delta t} =& \lambda e^{-j\beta_m \Delta x} + (1-2\lambda) + \lambda e^{j\beta_m \Delta x} \\
e^{\gamma \Delta t} =& 1 - 2\lambda \left(1 - \frac{e^{j\beta_m \Delta x} + e^{-j\beta_m \Delta x}}{2}\right) \\
e^{\gamma \Delta t} =& 1 - 2\lambda \left(1 - \cos\left(\beta_m \Delta x\right)\right) \\
e^{\gamma \Delta t} =& 1 - 4\lambda \sin^2\left(\frac{\beta_m \Delta x}{2}\right).
\end{aligned}
$$

Though these exponential factors are not the same as the eigenvalues in equation (1.14), they do give the same bounds on error growth in time as the eigenvalues.

When the PDE is defined with Neumann, $\frac{\partial u}{\partial x}|_{\Gamma_l} = \alpha_l$, or Robin, $\alpha_l u|_{\Gamma_l} + \beta_l \frac{\partial u}{\partial x}|_{\Gamma_l} = \gamma_l$, boundary conditions for boundary l, the matrix form

$$
A = \begin{bmatrix}
a + \sqrt{bc} & c & & 0 \\
b & a & \ddots & \\
 & \ddots & \ddots & c \\
0 & & b & a + \sqrt{bc}
\end{bmatrix},
$$

may be applicable. This matrix has eigenvalues specified by

$$
\mu^{(i)} = a + 2\sqrt{bc}\, \cos\left(\frac{(i-1)\,\pi}{N}\right),\ i = 1, 2, \ldots, N
$$

and eigenvectors, $u^{(i)}$, specified in [41] by component k as

$$
\begin{aligned}
u_k^{(1)} &= \sqrt{\frac{b}{c}}^{k-1},\ k = 1, 2, ..., N \\
u_k^{(i)} &= \sqrt{\frac{b}{c}}^{k-1} \cos\left(\frac{(i-1)\,(2k-1)\,\pi}{2N}\right),\ i = 2, 3, \ldots, N,\ k = 1, 2, ..., N.
\end{aligned}
$$

For the forward Euler method for the heat equation with zero Neumann conditions,

$$\begin{aligned}\frac{\partial u}{\partial t} =& \frac{\partial^2 u}{\partial x^2},\\ u(x,0) =& u_0(x)\\ \frac{\partial u}{\partial x}(0,t) =& 0,\\ \frac{\partial u}{\partial x}(L,t) =& 0,\end{aligned}$$

the difference equation,

$$u^{n+1} = A_{EN} u^n,$$

has the matrix form,

$$A_{EN} = \begin{bmatrix} 1-\lambda & \lambda & & 0 \\ \lambda & 1-2\lambda & \ddots & \\ & \ddots & \ddots & \lambda \\ 0 & & \lambda & 1-\lambda \end{bmatrix},$$

for $\lambda = \frac{\Delta t}{\Delta x^2}$. Notice that with $a = 1-2\lambda$ and $b = c = \lambda$, the eigenvalues for A_{EN},

$$\mu^{(i)}(\lambda) = 1 - 4\lambda \sin^2\left(\frac{i\pi}{2N}\right),\ i = 1, 2, \ldots, N \tag{1.15}$$

are only slightly different from that of matrix A_{ED}, and the distinctly different corresponding eigenvectors are defined by component k as

$$\begin{aligned} u_k^{(1)} &= 1,\ k = 1, 2, ..., N\\ u_k^{(i)} &= \cos\left(\frac{(i-1)(2k-1)\pi}{2N}\right),\ i = 2, 3, \ldots, N,\ k = 1, 2, ..., N. \end{aligned}$$

Chapter 2

EXAMPLE APPLICATIONS

2.1 Degenerate Fitzhugh-Nagumo Equation

For this application, we will compare our operator splitting method to three full methods and see an example where the operator splitting solution can better approximate a traveling wave than the comparable full problem. Further, our operator splitting solution utilizes a two-level splitting to access the maximum number of exact solutions to split problems.

2.1.1 Modeling Nerve Impulses

We now consider the Fitzhugh-Nagumo system, which models the propagation of nerve signals along the axon of a neuron [25]. We will utilize the asymptotic solution for a particular form of this nonlinear system to provide absolute error measurement.

To test our various numerical methods, we will apply them to the one-dimensional degenerate form of the Fitzhugh-Nagumo system,

$$\begin{aligned} \frac{\partial u}{\partial t} &= \frac{\partial^2 u}{\partial x^2} + f(u), \quad -\infty < x < \infty, \\ \lim_{x\to\pm\infty} \frac{\partial u}{\partial x} &= 0, \quad u(x,0) = u_0(x) = \left[1 + e^{-x/\sqrt{2}}\right]^{-1}, \end{aligned} \tag{2.1}$$

where $f(u) = u(1-u)(u-a)$ for $0 < a < \frac{1}{2}$. This system, which governs the conduction of electrical impulses in a nerve axon, has been extensively studied for various initial and boundary conditions, and is found to have stable steady states at $u = 0$ and $u = 1$ and an unstable steady state at $u = a$ [25]. Note that we have chosen the initial conditions to match the initial state of the Huxley asymptotic solution [25],

$$u = \left[1 + e^{-\xi/\sqrt{2}}\right]^{-1}, \quad \xi = x + ct, \quad c = \sqrt{2}\left(\frac{1}{2} - a\right). \tag{2.2}$$

Given any initial or boundary conditions of this degenerate form of the Fitzhugh-Nagumo system, the limiting solution is a combination of bounded traveling waves determined by the Huxley solution. Matching our initial conditions to this asymptotic solution provides an exact solution of our nonlinear reaction diffusion equation.

2.1.2 Comparison of Various Methods

To simulate wave propagation, we discretize the model equation (2.1) through a finite window of the spatial domain. The endpoints, a and b, are to be chosen far enough away from the wave so that our finite boundary conditions do not interfere with the propagation of the wave. To match the second order approximation of the spatial diffusion, we determine the boundary conditions via a second order ghost point method. Note that we evaluate the approximation with nodes at the centers of the intervals. This allows for the boundary conditions to be determined by

$$u_{a-1}^n = u_a^n \quad \text{and } u_{b+1}^n = u_b^n.$$

To analyze our operator splitting method, we will not only compare it to the exact solution just described, but also to three different full, or standard, numerical methods. The first two will demonstrate an over- and under-approximation of the speed of the traveling wave. These are the implicit full and explicit full methods. The third is a predictor-corrector method, an explicit/implicit mixture which is most conceptually similar to our operator splitting method, the fourth method.

2.1.2.1 Implicit Full Method

An implicit scheme for the full semilinear PDE (2.1) gives the following discretized system of equations,

$$\frac{u_i^{n+1}-u_i^n}{\Delta t}=\frac{1}{\Delta x^2}\delta_x^2 u_i^{n+1}+f\left(u_i^{n+1}\right),$$

where $\delta_x^2 u_i^{n+1}=u_{i-1}^{n+1}-2u_i^{n+1}+u_{i+1}^{n+1}$. Since the discretization is looking backward in time, the implicit full solution will be slightly ahead of the exact wave solution as shown in figure 4. The nonlinearity of $f\left(u_i^{n+1}\right)$, however, forces us to apply some linearization in terms of the unknown variable, u_i^{n+1}, in order to invert the operator numerically. Notice, that by Taylor expansion, this linearization is actually second order in time,

$$\begin{aligned}
u_i^{n+1}\left(1-u_i^{n+1}\right)\left(u_i^{n+1}-a\right) =& f\left(u_i^{n+1}\right)\\
f\left(u_i^{n+1}\right) =& f\left(u_i^n+\left(u_i^{n+1}-u_i^n\right)\right)\\
=& f\left(u_i^n\right)+\left(u_i^{n+1}-u_i^n\right)f'\left(u_i^n\right)+\left(u_i^{n+1}-u_i^n\right)^2 f''\left(u_i^n\right)+O\left(\left(u_i^{n+1}-u_i^n\right)^3\right)\\
=& f\left(u_i^n\right)+\left(u_i^{n+1}-u_i^n\right)f'\left(u_i^n\right)+\left(\Delta t\frac{\partial u_i^n}{\partial t}+O\left(\Delta t^2\right)\right)^2 f''\left(u_i^n\right)+O\left(\left(u_i^{n+1}-\right.\right.\\
=& u_i^{n+1}f'\left(u_i^n\right)+\left(f\left(u_i^n\right)-u_i^n f'\left(u_i^n\right)\right)+O\left(\Delta t^2\right),
\end{aligned}$$

where $f'=\frac{\partial f}{\partial u}$. Since this linearization couples u^n and u^{n+1}, the matrix needs to be updated at each time step. Hence, while second order, the linearization preserves the method's order one accuracy in time. The inner solution of the approximate system is then written as

$$\begin{aligned}
-\lambda u_{i-1}^{n+1}+\left[1+2\lambda-\Delta t f'\left(u_i^n\right)\right]u_i^{n+1}-\lambda u_{i+1}^{n+1} &= u_i^n+\Delta t[f\left(u_i^n\right)-u_i^n f'\left(u_i^n\right)]\\
B_2 u^{n+1} &= u^n+\Delta t[f\left(u_i^n\right)-u^n f'\left(u_i^n\right)], \quad (2.3)
\end{aligned}$$

where $\lambda=\frac{\Delta t}{\Delta x^2}$ and matrix B_2 is

$$B_2 = \begin{bmatrix} 1+\lambda-\Delta t f'(u_1^n) & -\lambda & 0 \\ -\lambda & 1+2\lambda-\Delta t f'(u_i^n) & \ddots \\ 0 & \ddots & 1+\lambda-\Delta t f'(u_m^n) \end{bmatrix}. \tag{2.4}$$

Notice how the ghost point condition coupled with having the nodes at interval centers diminishes the main diagonal term on the boundaries of the B_2 matrix 2.4.

2.1.2.2 Explicit Full Method

An explicit discretization of the full equation,

$$\frac{u_i^{n+1}-u_i^n}{\Delta t} = \frac{1}{\Delta x^2}\delta_x^2 u_i^n + f(u_i^n),$$

preserves a simple computation on the right hand side using known information. As this discretization is looking forward in time, the explicit full solution will be slightly behind the exact wave solution as shown in figures 4 and 5,

$$\begin{aligned} u_i^{n+1} &= \lambda u_{i-1}^n + (1-2\lambda)u_i^n + \lambda u_{i+1}^n + \Delta t u_i^n(1-u_i^n)(u_i^n - a), \\ u^{n+1} &= A_1 u^n + \Delta t u^n(1-u^n)(u^n - a), \end{aligned}$$

where

$$A_1 = \begin{bmatrix} 1-\lambda & \lambda & 0 \\ \lambda & 1-2\lambda & \ddots \\ 0 & \ddots & 1-\lambda \end{bmatrix}. \tag{2.5}$$

As with the implicit matrix (2.4), the ghost point approximation also diminishes the main diagonal term of the explicit A_1 matrix (2.5).

2.1.2.3 Explicit Split Method

Now we consider a splitting method that decouples the semilinear operator. The operator will be split so as to solve two separate PDEs which are cheaper to solve. Specifically, we split the reaction and diffusion parts of the full equation (2.1) into the split equations,

$$\frac{1}{2}\frac{\partial u}{\partial t} = u(1-u)(u-a), \tag{2.6}$$

$$\frac{1}{2}\frac{\partial u}{\partial t} = \frac{\partial^2 u}{\partial x^2}, \tag{2.7}$$

solved sequentially over the subintervals $\left\{\left[t_n, t_n + \frac{\Delta t}{2}\right], \left[t_n + \frac{\Delta t}{2}, t_n + \Delta t\right]\right\}$, where $t_{n+1} = t_n + \Delta t$. Since the exact solution for the reaction split equation (2.6) cannot be written explicitly for a general $0 < a < 1/2$, we solve it numerically using an explicit method,

$$u_i^{n+\frac{1}{2}} = u_i^n + 2\Delta t u_i^n \left(1 - u_i^n\right)\left(u_i^n - a\right),$$

where $u_i^{n+\frac{1}{2}} = u\left(x_i, t_{n+\frac{1}{2}}\right)$. To match the accuracy of the full methods, and to simulate a split version of the explicit full method, the diffusion split equation (2.7) is solved via the explicit Euler method,

$$u^{n+1} = A_2 u^n, \tag{2.8}$$

where

$$A_2 = \begin{bmatrix} 1-2\lambda & 2\lambda & 0 \\ 2\lambda & 1-4\lambda & \ddots \\ 0 & \ddots & 1-2\lambda \end{bmatrix}. \tag{2.9}$$

Since this numerical solution is first order in time, any splitting accuracy higher than first order would be lost after the diffusion step, this $O(\Delta t)$ accuracy is maintained by

the chosen split recombination to obtain the global explicit split solution over the interval $\{[t_n, t_{n+1}]\}$. The theoretical accuracy of this first order split recombination scheme is proven by theorem 1.1 in subsection 1.1.4.

2.1.2.4 Explicit Double Split Method

Now we consider a splitting method that decouples the semilinear operator further to access exact solutions for the reaction split equation. Since the exact solution for the reaction split equation (2.6) cannot be written explicitly for a general $0 < a < 1/2$, we rewrite $a = \frac{1}{2} - \left(\frac{1}{2} - a\right)$, where the exact solution for (2.6) is known when $a = \frac{1}{2}$. Applying this substitution, we further split the reaction equation (2.6),

$$\begin{aligned}\frac{1}{2}\frac{\partial u}{\partial t} =& u(1-u)(u-a)\\ =& u(1-u)\left(u - \frac{1}{2}\right) + \left(\frac{1}{2} - a\right)u(1-u),\end{aligned}$$

into the two PDEs,

$$\frac{1}{4}\frac{\partial u}{\partial t} = \left(\frac{1}{2} - a\right)u(1-u), \tag{2.10}$$

$$\frac{1}{4}\frac{\partial u}{\partial t} = u(1-u)(u - \frac{1}{2}), \tag{2.11}$$

which are solved over the subintervals $\left\{\left[0, \frac{\Delta t}{4}\right], \left[\frac{\Delta t}{4}, \frac{\Delta t}{2}\right]\right\}$, and whose exact solutions can be written explicitly as

$$\begin{aligned}u_i^{n+1/4} &= \frac{u_i^n}{(1-u_i^n)\, e^{-\left(\frac{1}{2}-a\right)\Delta t} + u_i^n},\\ u_i^{n+1/2} &= \frac{1}{2} + \frac{\frac{1}{2}(u_i^{n+1/4} - \frac{1}{2})}{\sqrt{u_i^{n+1/4}(1-u_i^{n+1/4})e^{-\Delta t/2} + \left(u_i^{n+1/4} - \frac{1}{2}\right)^2}}.\end{aligned}$$

We sequentially solve reaction sub-splits (2.10), (2.11), and then diffusion split (2.7) within one global time step. Again, the diffusion split equation will be solved via the explicit Euler method (2.8). As with the previous split method, we maintain an $O(\Delta t)$ accuracy, this time by solving the set of split equations

$$\left\{ \frac{1}{4}\frac{\partial u}{\partial t} = \left(\frac{1}{2} - a\right) u(1-u),\ \frac{1}{4}\frac{\partial u}{\partial t} = u(1-u)\left(u - \frac{1}{2}\right),\ \frac{1}{2}\frac{\partial u}{\partial t} = \frac{\partial^2 u}{\partial x^2} \right\},$$

sequentially over the subintervals $\left\{ \left[t_n, t_n + \frac{\Delta t}{4}\right], \left[t_n + \frac{\Delta t}{4}, t_n + \frac{\Delta t}{2}\right], \left[t_n + \frac{\Delta t}{2}, t_n + \Delta t\right] \right\}$ to obtain the global explicit split solution over the interval $\{[t_n, t_{n+1}]\}$. The theoretical accuracy of this first order split recombination scheme is proven by applying theorem 1.1 in subsection 1.1.4 to both first order split recombinations of equations (2.6) and (2.7), then to further recombination of reaction splits (2.10) and (2.11) .

2.1.2.5 Note on Disguised Split Methods

Though we will not compare the solution of this next method, we include it as an example of operator splitting under disguise. Since linearization restricts the accuracy of an implicit method from the outset, we may wish to consider the semi-implicit method,

$$u_i^{n+1} - \lambda \delta_x^2 u_i^{n+1} = u_i^n + \Delta t f\left(u_i^n\right),$$

where $\delta_x^2 = u_{i-1} - 2u_i + u_{i+1}$ is the standard second order central differencing, for our governing equation (2.1). Essentially, this method discretizes the linear diffusion operator implicitly and the nonlinear reaction operator explicitly. If, however, we were to split the governing equation as

$$\frac{1}{2}\frac{\partial u}{\partial t} = f(u),$$
$$\frac{1}{2}\frac{\partial u}{\partial t} = \frac{\partial^2 u}{\partial x^2},$$

and solve the nonlinear reaction split explicitly over the subinterval $\left[t_n, t_{n+1/2}\right]$ and solve the linear diffusion split implicitly over the subinterval $\left[t_{n+1/2}, t_{n+1}\right]$, in correspondence to the definition of the semi-implicit method, we obtain the combined method

$$\begin{aligned} u_i^{n+1} - \lambda\delta_x^2 u_i^{n+1} =& u_i^{n+1/2} \\ =& u_i^n + \Delta t f\left(u_i^n\right), \end{aligned}$$

where $\lambda = \frac{\Delta t}{\Delta x^2}$. Notice that the semi-implicit full and semi-implicit split methods are exactly the same. Hence, though the construction of split methods is a stark contrast to standard numerical methods, the computations involved may be quite similiar.

2.1.3 Accuracy and Stability Analysis

Using a second order central difference approximation in space and first order time solution approximations, one can see clearly that the implicit full and explicit full methods are $O\left(\Delta t + \Delta x^2\right)$ accurate. As the predictor-corrector method is an average of two explicit Euler methods, it is also $O\left(\Delta t + \Delta x^2\right)$ accurate. The explicit split method has $O\left(\Delta t + \Delta x^2\right)$ error in the explicit diffusion solution, no error in the reaction sub-split solutions, and $O\left(\Delta t\right)$ combined splitting error, so it is also a $O\left(\Delta t + \Delta x^2\right)$ accurate method.

Stability analysis of nonlinear methods is approximate at best. Because there is no way of calculating the changing eigenvalues of these systems, we will use an adapted Von Neumann analysis to determine stability conditions of the linearized form of the methods. We will first try to bound the error factor as usual, $\left|e^{\gamma \Delta t}\right| < 1$, but if that fails, we will look at the approximate form from definition 1.4, which bounds the error factor below the linearized exponential.

For the implicit full method, if we linearize the nonlinear terms and freeze their nonlinear components, the inner solution error reduces to

$$\begin{aligned} e^{\gamma \Delta t} &= \frac{1 + \Delta t \left(\frac{f\left(u_i^n\right)}{u_i^n} - f'\left(u_i^n\right) \right)}{1 + 4\lambda \sin^2\left(\frac{\beta \Delta x}{2}\right)} \\ &= \frac{1 - \Delta t \left(1 + a\right) u_i^n + 2\Delta t \left(u_i^n\right)^2}{1 + 4\lambda \sin^2\left(\frac{\beta \Delta x}{2}\right)}. \end{aligned}$$

Using our feasibility bounds, $0 < a < \frac{1}{2}$ and $0 < u_i^n < 1$, and directly computing the minimum of the numerator as a quadratic and evaluating the end points, we obtain the bounds

$$1 - \frac{(1+a)^2}{8}\Delta t < 1 - \Delta t \left(1 + a\right) u_i^n + 2\Delta t \left(u_i^n\right)^2 < 1 + \Delta t \left(1 - a\right), \tag{2.12}$$

and evaluating the denominator at the critical points $\beta = k\pi$ for any integer k, we obtain the bounds

$$1 \leq 1 + 4\lambda \sin^2\left(\frac{\beta \Delta x}{2}\right) < 1 + 4\lambda.$$

Since $1 + \Delta t(1 - a) \not\leq 1$ for feasible values of a, we cannot obtain a condition for strict stability, so we seek an approximate stability condition of the form $\left|e^{\gamma \Delta t}\right| < 1 + \Delta t$. Multiplying through by the denominator of the error factor, the approximate stability

condition we seek takes the form,

$$-1-\Delta t-4\lambda\left(1+\Delta t\right)\sin^2\left(\frac{\beta\Delta x}{2}\right)<1-\Delta t\left(1+a\right)u_i^n+2\Delta t\left(u_i^n\right)^2,\text{ and} \tag{2.13}$$

$$1-\Delta t\left(1+a\right)u_i^n+2\Delta t\left(u_i^n\right)^2<1+\Delta t+4\lambda\left(\Delta t+1\right)\sin^2\left(\frac{\beta\Delta x}{2}\right). \tag{2.14}$$

The right-hand term of inequality (2.14) has a minimum of $1+\Delta t$ when $\beta=2k\pi$ for any integer k, while the central term, which is the numerator of the error factor, has a maximum of $1+\Delta t(1-a)$, as computed in (2.12). Due to the feasibility bounds on a, the right inequality of (2.12) holds with no condition on the step sizes. The left-hand term of inequality (2.13) has a maximum of $-1-\Delta t$ when $\beta=2k\pi$ for any integer k, while the minimum of the central term is $1-\frac{(1+a)^2}{8}\Delta t$, as computed in (2.12). Due to the feasibility bounds on a, this quadratic minimizes at $1-\frac{9}{32}\Delta t$ when $a=\frac{1}{2}$. This minimum never reaches $-1-\Delta t$, and only reaches -1 with an infeasibly large time step, $\Delta t=\frac{64}{9}$. Hence, the left inequality of (2.12) holds with no condition on the step sizes.

Thus, $\left|e^{\gamma\Delta t}\right|<1+\Delta t$ without condition so the implicit full method is unconditionally approximately stable. Further, applying the loose bound $\Delta t<\frac{64}{9}$, the error factor is further restricted to $0<e^{\gamma\Delta t}<1+\Delta t$, so the method is also oscillation-free.

For the explicit full method, the inner solution error reduces to

$$e^{\gamma\Delta t}=1-4\lambda\sin^2\left(\frac{\beta\Delta x}{2}\right)+\Delta t f_2\left(u_i^n\right).$$

Using further feasibility bounds, $-\frac{1}{2}<f_2\left(u_i^n\right)<\frac{1}{4}$, where $f_2\left(u_i^n\right)=\frac{f\left(u_i^n\right)}{u_i^n}=\left(1-u_i^n\right)\left(u_i^n-a\right)$, the error factor cannot be bounded above by 1. Since

$$1-4\lambda-\frac{\Delta t}{2}<1-4\lambda\sin^2\left(\frac{\beta\Delta x}{2}\right)+\Delta t f_2\left(u_i^n\right)<1+\frac{\Delta t}{4},$$

however, we can apply the approximate stability condition $\lambda < \frac{1}{2}$ or $\Delta t < \frac{\Delta x^2}{2}$, to obtain the bound

$$-1 - \Delta t < e^{\gamma \Delta t} < 1 + \Delta t.$$

If we further restrict $\Delta t < \frac{2\Delta x^2}{\Delta x^2 + 8} < \frac{\Delta x^2}{2}$, then

$$0 < e^{\gamma \Delta t} < 1 + \Delta t,$$

making the method oscillation-free as well as approximately stable.

For the explicit split method, where split solutions are combined sequentially, the stability of the method as a whole depends exactly on the stability of the split equations independently. The error factor for the reaction split reduces to

$$e^{\gamma \Delta t} = 1 + 2\Delta t f_2\left(u_i^n\right).$$

Again using the feasibility bounds, $-\frac{1}{2} < f_2\left(u_i^n\right) < \frac{1}{4}$, to obtain the inequalities

$$1 - \Delta t < 1 + \Delta t f_2\left(u_i^n\right) < 1 + \frac{\Delta t}{2},$$

which satisfies the approximate stability bounds for $e^{\gamma \Delta t}$. If we choose $\Delta t < 1$, our reaction split solution is also oscillation-free. Since the diffusion split equation has zero Neumann boundary conditions (2.1), we can use the matrix form (1.11) for matrix A_2 (2.9) by replacing λ with 2λ, to compute the eigenvalues of A_2, directly with equation (1.15) as

$$\mu_i = 1 - 8\lambda \sin^2\left(\frac{i\pi}{2N}\right), \; i = 1, ..., N.$$

Without any need for feasibility bounds or approximate stability checks, if we force $\lambda < \frac{1}{4}$ or $\Delta t < \frac{\Delta x^2}{4}$, then $|\mu_i| < 1$ for all i, making the diffusion split solution stable. Further, if we force $\Delta t < \frac{\Delta x^2}{8}$, then we have positive eigenvalues, $0 < \mu_i < 1$, making the diffusion split solution oscillation-free. Combining the stability bounds for both split solutions, if $\Delta t < \min\{\frac{\Delta x^2}{8}, 1\}$, then our explicit split solution is oscillation-free and approximately stable.

For the explicit double split method, where split solutions are again combined sequentially, the stability of the method as a whole depends again on the stability of the split equations independently. Since the reaction sub-split equations are solved exactly, we need to only check the diffusion split solution for stability. Since the diffusion split is solved exactly as with the explicit split solution, the same stability bounds apply. Thus, if we force $\Delta t < \frac{\Delta x^2}{8}$, then we have positive and bounded eigenvalues, $0 < \mu_i < 1$, making the explicit double split method oscillation-free and stable. Note that the stability of the explicit double split method is more strictly defined than for the explicit split method.

In further applications, we will solve the linear diffusion split equation implicitly, because the implicit method, also known as the backward Euler method, is unconditionally oscillation-free and stable for linear problems, unlike the implicit full method (2.3) which is applied to the semilinear PDE (2.1).

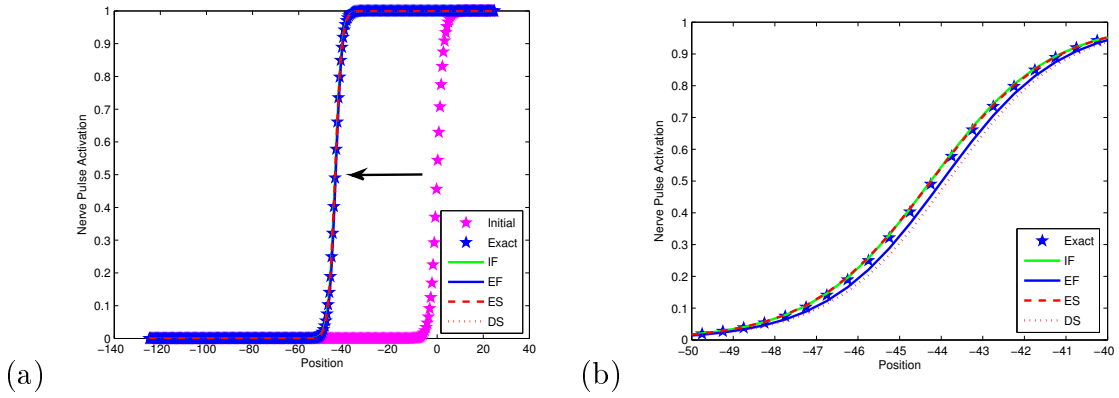

Figure 4: Comparison of the exact and four numerical solutions to equation 2.1 at $t = 125$: Exact asymptotic (Exact), implicit full (IF), explicit full (EF), explicit split (ES), and explicit double split (DS) solutions. Subplot (a) shows the whole domain used, while (b) shows a zoomed-in view of the traveling wave.

2.1.4 Results

A comparison of the exact asymptotic solution to all five numerical solutions are demonstrated in figure 4. While the explict full and explicit double split solutions are right-leaning, under-approximations, it makes sense that the implicit full method is a left-leaning, over-approximation to the left-traveling wave, but so is the explicit split method. This is indeed strange, as both splits in this method are solved explicitly, so the solution should be dragging in time like the other explicit methods. Also, notice that the explicit split solution is considerably better than the explicit full solution, even though the only difference between the two is the operator splitting itself.

Direct comparison between numerical solutions is more clear in the zoomed-in frame 4(b). It is clear that the explicit split solution is more accurate than the explicit full solution, specifically. Though both methods have the same order accuracy, we deduce that the additional splitting error is counteracting part of the error generated by the explicit solution. This is not true in general, as shown by the explicit double split solution.

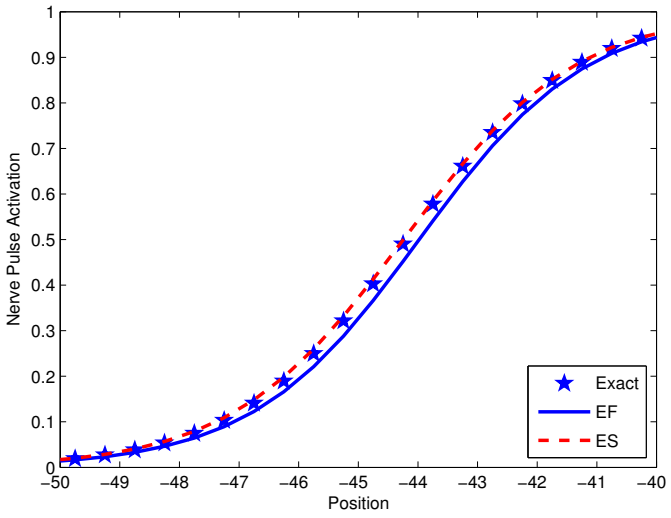

Figure 5: Comparison of exact asymptotic (Exact), explicit full (EF), and explicit split (ES) solutions to the Fitzhugh-Nagumo equation at $t = 125$.

Though it has exact solutions to the reaction sub-split equations, it is less accurate than the explicit split solution which explicitly approximates the reaction solution. This loss of accuracy is probably due to the additional splitting employed by the explicit double split method.

Since the explicit full and explicit split methods are so closely related, we contrast them specifically in figure 5. To better gauge the accuracy of these two methods corresponding to a traveling wave, we can compute the quantitative error in two meaningful ways. First, we can compute the two-norm error at $t = 125$ seconds across the whole discretized domain,

$$\|u_E - u_{EF}\|_2 = 0.080,$$

$$\|u_E - u_{ES}\|_2 = 0.016,$$

and see that the split solution accrues less error across the domain. Second, we can compute the wave speed of each method. By using the transformation, $z = x + ct$, the governing PDE (2.1) can be rewritten, integrated, and simplified using the boundary conditions and initial condition behavior as

$$\begin{aligned} u_t &= u_{xx} + f(u), \\ \int_{-\infty}^{\infty} cu' dz &= \int_{-\infty}^{\infty} (u'' + f(u))\, dz, \\ cu\big|_{-\infty}^{\infty} &= u'\big|_{-\infty}^{\infty} + \int_{-\infty}^{\infty} f(u) dz, \\ c &= \int_{-\infty}^{\infty} f(u) dz \\ &= \int_{-\infty}^{\infty} u(1-u)\,(u-a)\, dz. \end{aligned}$$

Hence, the approximate wave speed can be computed by

$$c = \int_{-A}^{B} u\,(1-u)\,(u-a)\, dx,$$

where $-A$ and B are set far enough away from the wave to approximately represent an infinite domain, the integration is sufficient over x, and the exact wave speed, $c = \sqrt{2}\left(\frac{1}{2} - a\right)$, is specified by the asymptotic solution (2.2). For $a = \frac{1}{4}$, the exact wave speed is $c = \frac{\sqrt{2}}{4} \approx 0.35355$. As the wave is traveling horizontally, a horizontal measure of error would seem more reasonable than a vertical measure of error, such as the two-norm error previously computed.

A comparison of these approximate and exact wave speeds is shown in figure 6. After convergence, their relative wave speed (RWS) errors are

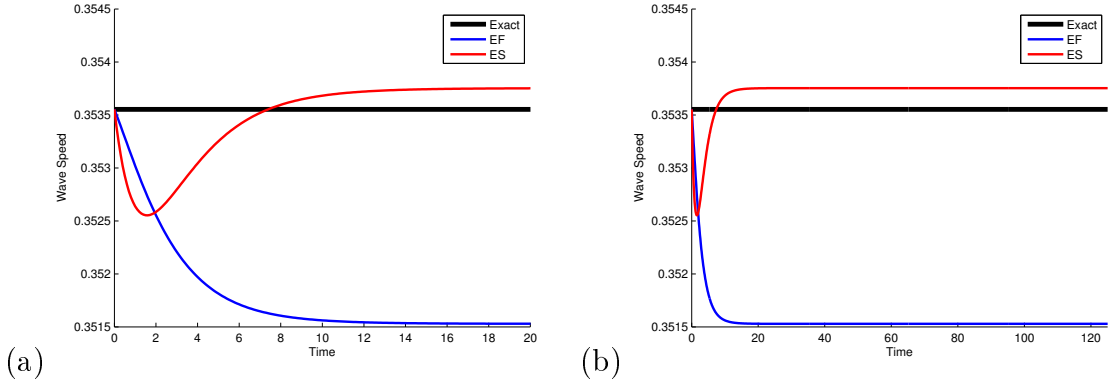

(a) (b)

Figure 6: Comparison of wave speeds for exact (Exact), explicit full (EF), and explicit split (ES) solutions. Sub-figures show (a) initial wave speeds at 20 seconds and (b) convergent wave speed approximations after 125 seconds.

$$\|u_E - u_{EF}\|_{RWS} = 0.42\%,$$

$$\|u_E - u_{ES}\|_{RWS} = 0.10\%.$$

It is clear, again, that the explicit split solution better approximated the wave speed than the explicit full solution. Interestingly enough, the split solution's approximation seems worse than the full solution initially, but then corrects itself to converge to a better wave speed approximation.

2.2 Fisher-Type Equation

For this application, we will utilize our splitting method in an investigation of oscillatory behavior in another semilinear reaction-diffusion equation. Further, the accuracy to our operator splitting solution, which is proven theoretically in subsection 1.1.4, is verified numerically by considering the numerical convergence of the solution in space and time as the respective mesh is refined by doubling the number of nodes at each step.

2.2.1 Modeling Spatially-Bounded Logistic Growth

In this section we will implement our proposed method on a Fisher-type equation defined on a bounded domain,

$$\begin{aligned} \frac{\partial u}{\partial t} &= \frac{\partial^2 u}{\partial x^2} + u(1-u),\ 0 < x < 10, \\ & u(0,t) = 0, \qquad u(10,t) = 0 \\ & u(x,0) = \frac{1}{100} + \frac{99}{100}\sin\left(\frac{\pi x}{L}\right). \end{aligned} \tag{2.15}$$

As an initial boundary value problem, the Fisher-type equation represents a logistic growth model [23]. The Fisher, or Fisher-Kolmogorov, equation is traditionally an initial value problem, and as such can model the propagation of a mutant gene, and flame propagation [16, 21].

Since data measurement introduces error beyond that considered for the computations, it is significant to consider its impact on numerical solutions. To represent a small measurement error in this specific Fisher-type equation, we defined the initial condition to create a slight discrepancy with the zero Dirichlet boundary conditions. This discrepancy causes the initial boundary value problem to be ill-posed, which means that there can be no continuous exact solution, so we desire a method that completely dampens out the discontinuity between the initial and boundary conditions.

2.2.2 Operator Splitting Implementation

As we are interested in comparing our operator splitting method to the Crank-Nicolson (CN) method, which has $O\left(\Delta t^2 + \Delta x^2\right)$ accuracy, we will utilize the second order split recombination from theorem 1.2. Accordingly, the governing equation is split,

$$\frac{1}{4}\frac{\partial u}{\partial t}+\frac{1}{2}\frac{\partial u}{\partial t}+\frac{1}{4}\frac{\partial u}{\partial t}=\frac{1}{2}u(1-u)+\frac{\partial^2 u}{\partial x^2}+\frac{1}{2}u(1-u),$$

into nonlinear reaction,

$$\frac{1}{4}\frac{\partial u}{\partial t}=\frac{1}{2}u(1-u), \tag{2.16}$$

and linear diffusion,

$$\frac{1}{2}\frac{\partial u}{\partial t}=\frac{\partial^2 u}{\partial x^2}, \tag{2.17}$$

split problems, which are recombined as the set of split equations,

$$\left\{\frac{1}{4}\frac{\partial u}{\partial t}=\frac{1}{2}u(1-u),\frac{1}{2}\frac{\partial u}{\partial t}=\frac{\partial^2 u}{\partial x^2},\frac{1}{4}\frac{\partial u}{\partial t}=\frac{1}{2}u(1-u)\right\},$$

which are solved over the set of subintervals

$$\left\{\left[t_n,t_{n+\frac{1}{4}}\right],\left[t_{n+\frac{1}{4}},t_{n+\frac{3}{4}}\right],\left[t_{n+\frac{3}{4}},t_{n+1}\right]\right\}.$$

2.2.3 Exact Reaction Solution

Here the reaction equation (2.16) is solved exactly. We have

$$\frac{du}{u(1-u)}=2dt.$$

Integrating it from t_n to $t_n=t_n+\triangle t$, we obtain,

$$\int_{u(x,t_n)}^{u(x,t_{n+1})}\left(\frac{1}{u}+\frac{1}{1-u}\right)du=2\int_{t_n}^{t_{n+1}}dt,$$

which gives

$$\ln \frac{u\left(x, t_{n+1}\right)}{1-u\left(x, t_{n+1}\right)}-\ln \frac{u\left(x, t_{n}\right)}{1-u\left(x, t_{n}\right)}=2 \triangle t.$$

Therefore, we obtain its exact solution,

$$u\left(x, t_{n+1}\right)=\left[1+\frac{1-u\left(x, t_{n}\right)}{u\left(x, t_{n}\right)} e^{-2 \triangle t}\right]^{-1}.$$

2.2.4 Oscillation-Free Method Comparison

The CN method is a widely used, unconditionally stable scheme for linear problems. Yet, this method can introduce oscillation and sometimes instabilities in the solution of semilinear problems similar to (1.4). In order to prohibit such oscillations we introduce a custom implicit scheme for the diffusion term, which is not only oscillation-free and unconditionally stable, but also has the same order of accuracy as the CN method.

2.2.4.1 Weighted Backward Scheme

For the diffusion split equation (2.17), written in spatially discretized operator form as

$$\frac{1}{2}\frac{\partial u}{\partial t} = Du,$$

the exact solution for the specified time interval is

$$u_E^{n+\frac{3}{4}} = e^{\Delta t D} u^{n+\frac{1}{4}},$$

where the exponential factor can be expanded as

$$e^{\Delta t D} = I + \Delta t D + \frac{\Delta t^2}{2} D^2 + \frac{\Delta t^3}{6} D^3 + O(\Delta t^3). \tag{2.18}$$

The diffusion equation could also be discretized with backward Euler method. From the exact solution $e^{-\Delta t D} u^{n+\frac{3}{4}} = u^{n+\frac{1}{4}}$, the first-order backward Euler method,

$$(I - \Delta t D)\, u^{n+\frac{3}{4}} = u^{n+\frac{1}{4}},$$

inverts as

$$u_F^{n+\frac{3}{4}} = (I - \Delta t D)^{-1} u^{n+\frac{1}{4}}. \tag{2.19}$$

By expanding the inverse factor,

$$(I - \Delta t D)^{-1} \;=\; I + \Delta t D + \Delta t^2 D^2 + \Delta t^3 D^3 + O(\Delta t^3), \tag{2.20}$$

and comparing it with the expansion of the exact solution (2.18), we can explicitly see its first-order accuracy in time as the order of agreement between the backward Euler and exact time solutions,

$$\begin{aligned} \left| u_F^{n+\frac{3}{4}} - u_E^{n+\frac{3}{4}} \right| &= \\ \left| \left[(I - \Delta t D)^{-1} - e^{\Delta t D} \right] u^{n+\frac{1}{4}} \right| &= \left| \frac{\Delta t^2}{2} D^2 u^{n+\frac{1}{4}} + O\left(\Delta t^3\right) \right| \\ &= O\left(\Delta t^2\right). \end{aligned}$$

Note that the expansion of the inverse is only valid when the spectral radius of $\Delta t D$ is less than one, that is, when $\Delta t < \frac{\Delta x^2}{4}$, where Δx is the spatial step used in the spatial discretization matrix, D.

The diffusion split equation(2.17) can also be discretized by splitting the diffusion operator itself,

$$\frac{1}{4}\frac{\partial u}{\partial t} + \frac{1}{4}\frac{\partial u}{\partial t} = \frac{1}{2} D u + \frac{1}{2} D u,$$

and solving both halves with separate implicit Euler methods. In other words, the

solution is obtained with two steps as

$$\begin{aligned} u^{n+\frac{1}{2}} &= (I - \frac{\Delta t}{2}D)^{-1}u^{n+\frac{1}{4}}, \\ u^{n+\frac{3}{4}} &= (I - \frac{\Delta t}{2}D)^{-1}u^{n+\frac{1}{2}}, \end{aligned}$$

or rewriting in the form,

$$u_H^{n+\frac{3}{4}} = (I - \frac{\Delta t}{2}D)^{-1}(I - \frac{\Delta t}{2}D)^{-1}u^{n+\frac{1}{4}}. \tag{2.21}$$

Again, we expand the inverse factors as

$$\begin{aligned} (I - \frac{\Delta t}{2}D)^{-1}(I - \frac{\Delta t}{2}D)^{-1} &= \left[I + \frac{\Delta t}{2}D + \frac{\Delta t^2}{4}D^2 + O(\Delta t^3)\right]^2 \\ &= I + \Delta t D + \frac{3}{4}\Delta t^2 D^2 + \frac{3}{8}\Delta t^3 D^3 + O(\Delta t^4). \end{aligned} \tag{2.22}$$

Comparing to the exact solution (2.18), it is clear that this two-step splitting has not increased the order of accuracy, namely, this combination of implicit Euler and exact time solutions both agree up to first order,

$$\begin{aligned} \left|u_H^{n+\frac{3}{4}} - u_E^{n+\frac{3}{4}}\right| &= \\ \left|\left[(I - \frac{\Delta t}{2}D)^{-1}(I - \frac{\Delta t}{2}D)^{-1} - e^{\Delta t D}\right]u^{n+\frac{1}{4}}\right| &= O\left(\Delta t^2\right). \end{aligned}$$

By weighting these two solutions, however, we can develop a custom implicit scheme with higher order accuracy. Two times solution (2.21) minus solution (2.19) gives the custom implicit discretization,

$$\begin{aligned} u_W^{n+\frac{3}{4}} &= 2u_H^{n+\frac{3}{4}} - u_F^{n+\frac{3}{4}} \\ &= \left(2(I - \frac{\Delta t}{2}D)^{-1}(I - \frac{\Delta t}{2}D)^{-1} - (I - \Delta t D)^{-1}\right)u^{n+\frac{1}{4}}. \end{aligned}$$

Following from equations (2.20) and (2.22), the weighted factor expands as

$$2(I - \frac{\Delta t}{2}D)^{-1}(I - \frac{\Delta t}{2}D)^{-1} - (I - \Delta t D)^{-1} = I + \Delta t D + \frac{v^2}{2}D^2 - \frac{\Delta t^3}{4}D^3 + O(\Delta t^3)$$

Comparing with the expansion of the exact solution (2.18), the weighted method approximates the exact solution up to second-order accuracy in time, since the two solutions differ at the third order,

$$\begin{aligned}\left|u_W^{n+\frac{3}{4}} - u_E^{n+\frac{3}{4}}\right| &= \left|\left(2(I-\frac{\Delta t}{2}D)^{-1}(I-\frac{\Delta t}{2}D)^{-1} - (I-\Delta tD)^{-1}\right)u^{n+\frac{1}{4}} - e^{\Delta tD}u^{n+\frac{1}{4}}\right| \\ &= O(\Delta t^3).\end{aligned}$$

For the spatial discretization of the diffusion operator, we set

$$D = \text{Tridiagonal}\left[\frac{1}{\Delta x^2}, -\frac{2}{\Delta x^2}, \frac{1}{\Delta x^2}\right],$$

such that the spatial accuracy is $O\left(\Delta x^2\right)$.

In sum, we have developed as weighed implicit scheme with a second-order accuracy in time and space, $O\left(\Delta t^2 + \Delta x^2\right)$, which is the same accuracy as the CN method but without the condition oscillatory behavior, as shown in section 2.2.4.2.

2.2.4.2 Oscillatory Behavior

The stability and oscillatory behavior of the weighted implicit scheme depends on the two Backward Euler schemes as weighted components. The two Backward Euler schemes are unconditionally stable and oscillation-free. To show it explicitly, we write equations (2.19) and (2.21) as

$$\begin{aligned}u^{n+\frac{3}{4}} &= [B(r)]^{-1}\, u^{n+\frac{1}{4}}, \\ u^{n+\frac{3}{4}} &= [B(r/2)]^{-1}\,[B(r/2)]^{-1}\, u^{n+\frac{1}{4}},\end{aligned}$$

where $B(r) = I - \Delta tD = \text{Tridiagonal}[-r, 1+2r, -r]$ with $r = \Delta t/\Delta x^2$. For this tridiagonal $N \times N$ matrix $B(r)$, its eigenvalues are,

$$\lambda_i(r) = 1 + 4r\cos^2\left(\frac{i\pi}{2\left(N+1\right)}\right),\ i = 1, 2, ..., N$$

and eigenvectors, $u^{(i)}$, specified by component k as

$$u_k^{(i)} = \sin\left(\frac{ik\pi}{N+1}\right),\ i = 1, 2, \ldots, N,\ k = 1, 2, ..., N$$

as long as we assume the first component is $u_1^{(i)} = \sin\left(\frac{i\pi}{N+1}\right),\ i = 1, 2, \ldots, N$ [41], as shown in section 1.2.2. Because the eigenvectors are independent of r, matrices $B(r)$ and $B(r/2)$ have the same eigenvectors allowing us to compute the eigenvalues of the weighted combination of these matrices, $[2B(r/2)B(r/2) - B(r)]^{-1}$, used in the weighted method as

$$\begin{aligned}
\mu_i(r) &= \left[2\lambda_i^2(r/2) - \lambda_i(r)\right]^{-1} \\
&= \left[\left(1 + 2r\cos^2\left(\frac{i\pi}{2N+2}\right)\right)^2 + 4r^2\cos^4\left(\frac{i\pi}{2N+2}\right)\right]^{-1},
\end{aligned}$$

for $i = 1, 2, ..., N$. Because $[\mu_i(r)]^{-1} \geq 1$, then $0 < \mu_i(r) \leq 1$, and hence the weighted scheme is not only unconditionally stable ($|\mu_i(r)| \leq 1$), but also unconditionally oscillation-free ($\mu_i(r) > 0$).

2.2.5 Results

To compare the oscillatory behavior of our weighted Euler and the CN method, we have implemented each as the method for solving the diffusion portion, keeping the exact solution for the reaction portion, and using the same alternating operator splitting scheme.

Figure 7 shows the results from these two schemes for spatial step, $\Delta x = 0.1$, and temporal step, $\Delta t = 0.2$. Figure 7(a) shows that in the CN scheme, initial perturbations at the boundaries propagate inward with subsequent iteration and introduce oscillations in the solution. This indicates that, though oscillations usually damp out over time for

a well-known stable method like CN, in combination with the nonlinearity and operator splitting, such oscillations blow up and thus destroy the stability superficially preserved by each solution step. Figure 7(b), however, shows that our weighted backwards Euler method is free from such oscillation, even given the same initial perturbation.

2.2.6 Accuracy Verification

To verify the accuracy of our method we have generated results by varying spatial meshes and temporal step. Table 1 demonstrates the second order accuracy in space and time. Since we have no exact solution to compare to, we measure the accuracy of our method by looking at the convergence of the difference between subsequent solutions as an indicator for the convergence of the numerical solution to the actual solution, which is the accuracy of the numerical method. In Table 1, the convergence rate is computed for each refinement of the mesh. For example, if a mesh step size is shrunk by a factor of m, for a second order method, we expect the solution difference to shrink correspondingly by a factor of m^2 [40].

Accuracy could be checked at any point in space or time, however, for longevity and ease of computation, we measure the spatial and temporal convergence of the solution for various meshes at $u(5, 25)$, which is the midpoint of the solution curve after a reasonable amount of time has passed. The spatial convergence, $\frac{|u_{H-1}-u_{H-2}|}{|u_H-u_{H-1}|}$, computes the shrinking factor between the solution improvement at the refined spatial step and that at the previous step, while the temporal convergence, $\frac{|u_{K-1}-u_{K-2}|}{|u_K-u_{K-1}|}$, computes the analogous factor for each refined time step. Here, u_H and u_K represent the solution, $u(5, 25)$, when the spatial mesh is $\Delta x = \frac{1}{2^H}$, and the temporal mesh is $\Delta t = \frac{1}{2^K}$, respectively. Both

H and K run from 0 up to 11, so that the mesh sizes Δx and Δt independently run from 1 down to $\frac{1}{2048}$, while the other mesh size is held fixed at 1. The left four columns show the convergence of the shrinking factor to 4 while the space step is shrunk by 2. Correspondingly, the right four columns show the convergence, albeit slower, of the shrinking factor to 4 while the time step is also shrunk by 2. This quadratic convergence, represented by $O\left(\Delta t^2 + \Delta x^2\right)$, is represented graphically in Figure 8.

Table 1: Numerical Verification of Accuracy at u(5,25)

H	Δx	Δt	$\frac{\lvert u_{H-1}-u_{H-2}\rvert}{\lvert u_H-u_{H-1}\rvert}$	Δx	K	Δt	$\frac{\lvert u_{K-1}-u_{K-2}\rvert}{\lvert u_K-u_{K-1}\rvert}$
0	1	1	$--$	1	0	1	$--$
1	$\frac{1}{2}$	1	$--$	1	1	$\frac{1}{2}$	$--$
2	$\frac{1}{4}$	1	4.233	1	2	$\frac{1}{4}$	3.223
3	$\frac{1}{8}$	1	4.051	1	3	$\frac{1}{8}$	4.200
4	$\frac{1}{16}$	1	4.013	1	4	$\frac{1}{16}$	4.931
5	$\frac{1}{32}$	1	4.003	1	5	$\frac{1}{32}$	5.246
6	$\frac{1}{64}$	1	4.001	1	6	$\frac{1}{64}$	5.118
7	$\frac{1}{128}$	1	4.000	1	7	$\frac{1}{128}$	4.785
8	$\frac{1}{256}$	1	4.000	1	8	$\frac{1}{256}$	4.473
9	$\frac{1}{512}$	1	4.000	1	9	$\frac{1}{512}$	4.261
10	$\frac{1}{1024}$	1	4.000	1	10	$\frac{1}{1024}$	4.138
11	$\frac{1}{2048}$	1	4.000	1	11	$\frac{1}{2048}$	4.062

2.3 Discussion

For both applications, we utilized exact solution(s) with our operator splitting methods. Not every semilinear equation can be split to allow access to an exact solution of the nonlinear portion, yet the splitting method can easily be applied to semilinear problems where the reaction portion cannot be solved exactly. In this case the numerical scheme

chosen must simply maintain the order of accuracy ensured by the other components of the method. Furthermore, this method need not be affixed to any certain type of problem. These two applications gave examples of both initial value and initial boundary value problems with Dirichlet and Neumann boundary conditions. This operator splitting method can be applied to a wide range of semilinear problems, as it worked equally well simulating traveling waves or spatially-bounded growth, and can easily accommodate mixed boundary conditions. Though this combination of operator splitting and oscillation-free techniques has been analyzed for semilinear equations, it may work just as well on nonlinear problems without diffusive terms.

Through these applications we demonstrated both first and second order splitting methods. Though the accuracy of our operator splitting method on a semilinear problem is proven in section 1.1.4, our conclusion is supported in section 2.2 by the numerical convergence verification of this accuracy in table 1.

In our first application, we compared two versions of our first order operator splitting method to two other standard methods for nonlinear equations, and saw that not only was the explicit split method accurate, it outperformed the standard explicit method. This is a fascinating, though not perpetual, occurrence as demonstrated by the comparison with the explicit double split method. Further, operator splitting can be easily nested, as shown in developing our explicit double split method for this initial value problem where we utilized splitting at two levels to access exact solutions.

In our next application, we developed an oscillation-free and unconditionally stable numerical scheme with second order accuracy in space and time to solve the semi-linear diffusion equation (1.4) and verified our claims theoretically and demonstrated their importance in figure 7. As data measurement is a major portion of simulation and

modeling real phenomena and measurement error is inevitable in practical problems, we made a point to make our problem inconsistent by forcing initial discrepancies at the boundaries. Stability is not the only condition for propagation of this initial error, though it is often the only one considered. We ran our method against the CN method to demonstrate the oscillations in the CN method and how our scheme eliminates these oscillations. Oscillations inherent in a numerical method are quickly exposed by even the slightest error, as our results for the CN method shown in figure 7(a), whereas oscillation-free methods remain unaffected by slight discrepancies and eventually damp out even large error, as demonstrated by the results for our method in figure 7(b).

It is important to note that, though the solution is second order accurate in space and time, the temporal convergence lags behind the spatial convergence. This shows that the operator splitting affects the convergence in time and has no effect on the convergence in space.

Figure 7: Comparing oscillatory behavior of (a) CN and (b) Weighted solutions to equation (2.15).

(a)

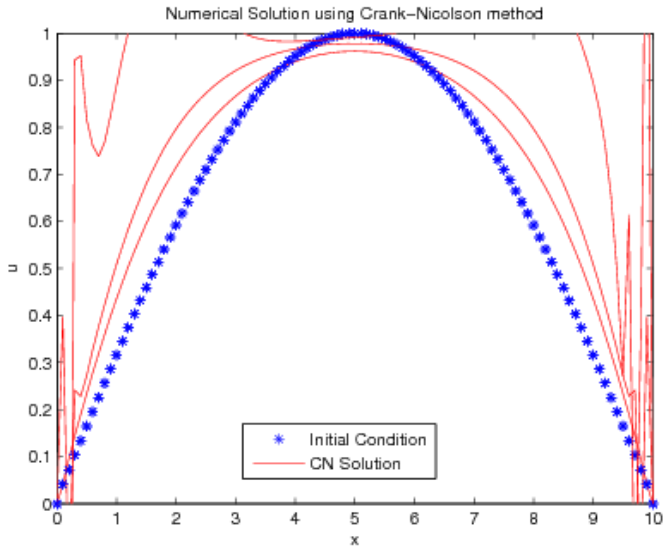

(b)

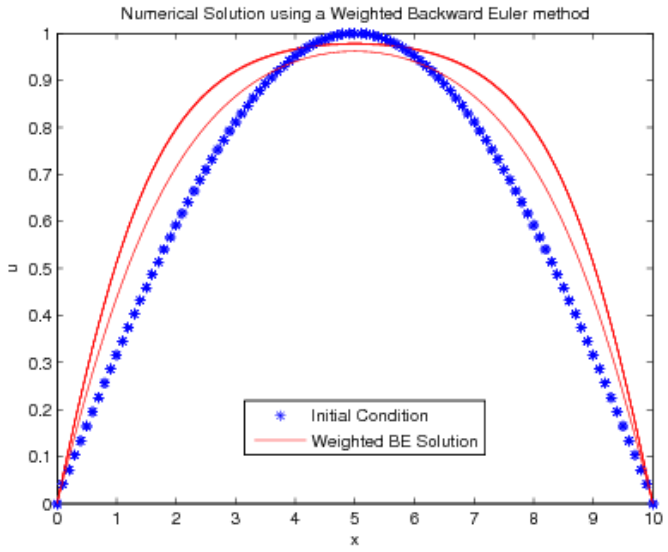

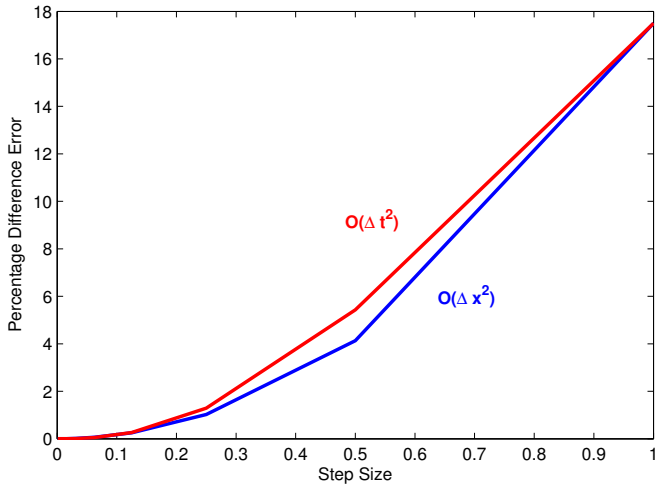

Figure 8: Graphical representation of quadratic convergence in space and time.

Chapter 3

LEAD-ACID BATTERY SIMULATION

3.1 Background for Lead-Acid Batteries

Demand for advancing vehicular technology has increased in recent years. At this time, there is a great need for better and cheaper hybrid and electric automobiles. Many factors have added to this growing need, including the high costs of petroleum, the volatile nature of its market, and the fear of its depleting sources, as well as global concern over carbon emissions. Over a ten year span from Jan. 2000 to Jan. 2010, U.S crude oil costs quadrupled, including a one-year doubling from 2007 to 2008 and one-year halving from 2008 to 2009 [11]. While demand held relatively steady over this decade [12], oil production faltered midway, decreasing for the first two consecutive years in 2006 and 2007 [13]. These trends are visualized in figure 9(a-c). Political and individual concerns over carbon emissions have greatly increased in recent years, because of health risks as well as current and future damage to the environment. Due to the combination of these factors and the anticipated benefits of alternate fuels, the need for research and development of alternate energy sources, specifically for personal transportation, is critical in manufacturing hybrid-electric vehicles.

Such research is being done, for example, at University of Idaho's Center for Intelligent Systems Research (CISR), where valve regulated lead-acid (VRLA) batteries are being designed and developed for optimal energy-to-weight ratios as an integral part of a complete electric vehicle system [1, 2, 7, 18, 42]. CISR is currently researching and developing an optimized VRLA battery designed to power electric vehicles [42]. This optimization research is aided by computer models of the electrochemical dynamics of proposed battery designs. This paper presents a model and a numerical method for simulating sulfuric acid diffusion in a VRLA battery. CISR has also been experimenting

(a)

(b)

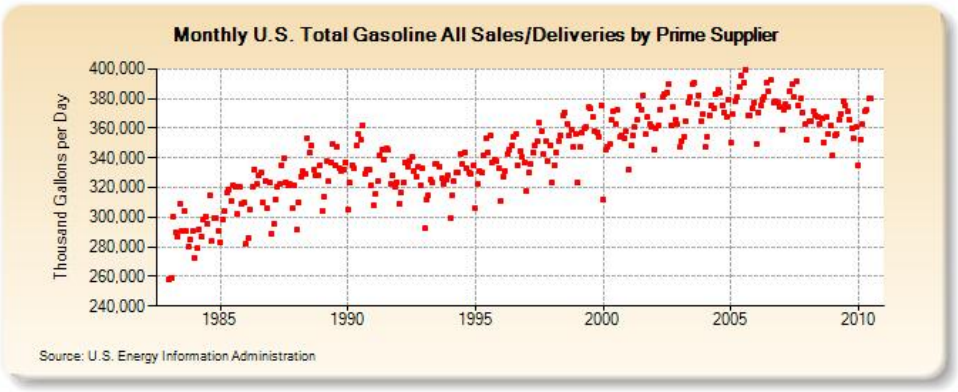

(c)

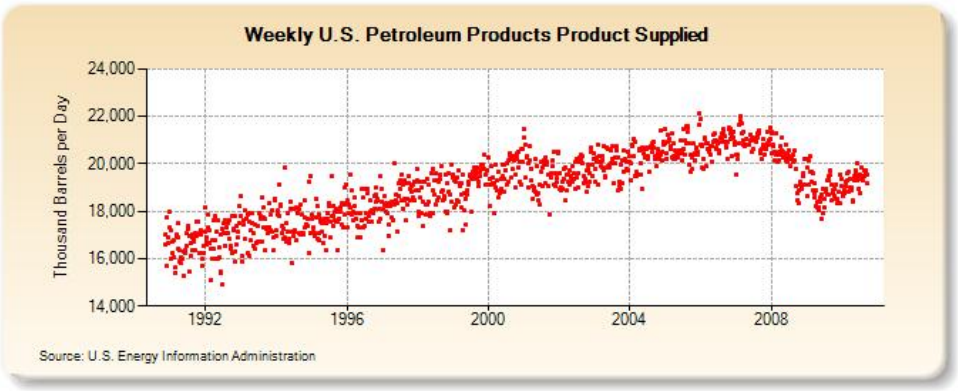

Figure 9: Trends for U.S. (a) spot oil prices FOB between 1978 and 2010 [11], (b) motor gasoline consumption between 1983 and 2010[12], and (c) amount of petroleum products supplied between 1990 and 2010 [13].

with conductive and nonconductive additives in the pastes that forms the electrodes. Conductive additives like titanium products may increase the utilization of the electrode [33] while nonconductive additives like hollow glass microspheres may increase the porosity, and thus acid storage in the plates [28]. Even when an additive assists one piece of the electrodes dynamics like controlling the hydrogen gassing, it's weight may adversely affect performance by decreasing utilization [3]. Thus, an additives benefits are weighed against their relevant costs.

This section presents a specifically simplified model and a numerical method for simulating sulfuric acid as it reacts and diffuses in a VRLA battery. Our contributions are as follows:

1. We construct a reaction-diffusion model $3.2 - 3.10$ for the concentration of sulfuric acid exclusively in a VRLA battery through relevant simplifying assumptions applied to the dynamical model 3.1 used in [37]. This new simplified model is analyzed and tested against experimental data.

2. We develop an operator splitting numerical method to split the given nonlinear PDE into an analytically solvable reaction step and a linear diffusion step. This splitting runs considerably faster than "real time" cited by [37], while maintaining consistency and stability. A demonstration of the computational run-times and the super-linear speed-up of our operator splitting method is shown in section 3.5.

3. We develop numerical schemes to preserve the first order in time and second order in space accuracy over the discontinuous interfaces. The interval centering discretization of the region avoids material interfaces where parameter values cannot be determined. See section 1.1.4 for theoretical proof and section 2.2.6 for example

A_j	electrode cross-sectional area in region $j = 1, 2, 3$
A_j^S	electrode active surface area per volume in region $j = 1, 2, 3$
b_j	simplifying reaction constant in region $j = 1, 2, 3$
c	concentration of sulfuric acid
c^0	initial sulfuric acid concentration
D	Reference diffusion rate
F	Faraday's constant: $F = 96,487$c/mol
f	mean molar activity coefficient for H_2SO_4
i	cell-pair current density
i^{app}	cell-pair discharge current density
i_j^0	exchange current density in electrode $j = 1, 3$
K_j	equivalent molarity to charge constant in electrode $j = 1, 3$
L_j	thickness of region $j = 1, 2, 3$
R	universal gas constant: $R = 8.3145$J/(mol K)
r	bulk cell resistance
t^+	transference number for H^+ions
u	electrode utilization
u_j^{CVF}	critical volume fraction in electrode $j = 1, 3$
V	battery voltage
W_j	weight of active material in electrode $j = 1, 3$
α_j	anodic transfer coefficient in electrode $j = 1, 3$
ε_j	porosity: volume fraction of region $j = 1, 2, 3$filled with acid
κ_j	charge density for electrode $j = 1, 3$
η_j	surface overpotential of electrode $j = 1, 3$

Table 2: Table of Symbols

numerical verification.

4. We calculate battery voltage from our sulfuric acid concentration using the Nernst equation [5], and then compare this calculated voltage to measured data from first discharge tests of similarly manufactured batteries. Due to high variability in this data, we further calibrate the model to match.

Background information concerning design, material properties, chemical properties

of lead-acid batteries are presented in subsections 3.1.1−3.1.3. Previous models and battery simulation research are described in subsection 3.1.4. The general diffusion model is developed in section 3.2 along with descriptions and justifications for assumptions leading to our simplified model. In section 3.4, the numerical method is described and analyzed for accuracy and stability. The list of parameter values and model calibration, including the derivation of the modified Nernst equation, are discussed in section 3.5. Section 3.5.2 then presents results of the numerical solution, both simulated concentration and computed voltage enabling direct comparison with measured voltage data. These results are then discussed in section 3.6.

3.1.1 Battery Design

In general, a VRLA battery is a combination of battery cells, where each cell is composed of an alternating stack of negative and positive electrodes, separated by a highly porous sheath called the separator, and saturated with sulfuric acid. A pressure sensitive release valve accompanies the outer casing to manage any gas created by the normal reactions. The basic design for the batteries used and constructed by CISR have six cells per battery and a sixteen negative–fifteen positive electrode stack in each cell. The electrodes are also called plates for their resemblance to solid metal plating once dried. An absorptive glassmat separator is woven between the electrodes to provide a reservoir of acid required for the discharge process.

Each cell pair consisting of one negative electrode, one separator, and one positive electrode creates about two volts when discharging. To ensure high amperage, the positive or negative nodes of each electrode are connected in parallel, while the voltage

is maintained at roughly two volts per battery cell. Then, the positive and negative nodes of each cell are connected in series to obtain roughly twelve volts from the six cells. Thus, the tested batteries approximate normal car batteries in voltage [42].

3.1.2 Material Properties

As the name suggests, valve regulated lead-acid batteries are primarily composed of lead (Pb). In constructing VRLA batteries, CISR begins by mixing together lead oxide (PbO), water, and a little sulfuric acid (H_2SO_4). For the negative electrode, just a little lignum, carbon black, and a spongy expander ($< 1\%$ each by volume) are added. This paste is then clamped onto both sides of a lead alloy grid ($< 2\%$ calcium or alimony by volume), and left to set up in the curing process. This creates the two electrodes, each about 50% porous, where the pores are on average one micron in diameter. Essentially, the negative and positive electrodes are formed of the same material, except for the small fraction of additives to make the negative electrode a little more porous than the positive electrode. After the electrodes are cured, they are wrapped in the glassmat separator and packed into a nonreactive plastic case to maintain pressure on the electrodes. The glassmat separator is highly porous, roughly 90% porous, with pores of all sizes. The battery cell cases are then filled with sulfuric acid to saturate the electrodes and separator, and then quickly charged to full capacity before the brittle dried paste dissolves in the acid [42].

CISR has also been experimenting with conductive and non-conductive additives in the pastes that forms the electrodes. Conductive additives like titanium products increase the conductivity, and possibly the maximum utilization, of the electrodes [33]

while non conductive additives like hollow glass microspheres increase the porosity, and possibly extend the life of batteries under high-rate discharges due to increased acid storage in the electrodes [28]. Even when an additive assists one piece of the electrodes dynamics like controlling the hydrogen gassing, its weight may adversely affect performance by decreasing utilization [3].

3.1.3 Electrochemical Properties

When initially formed, the negative and positive electrodes are both primarily lead oxide (PbO). Once charged, they never return to this original composition. At full charge, the negative and positive electrodes are composed of lead (Pb) and lead dioxide (PbO_2) ions, respectively. By placing a load on the battery, the ions in both electrodes react with the sulfuric acid (H_2SO_4) to form lead sulfate ($PbSO_4$); diminishing the amount of sulfuric acid and diluting the solution with water (H_2O) and hydrogen gas (H) in each porous electrode. The discharge process is initiated by the current drawing electrons from the negative electrode. This loss of electrons in the presence of the sulfuric acid oxidizes the lead to lead sulfate while releasing hydrogen ions (gas).

$$Pb + HSO_4^- \rightleftharpoons PbSO_4 + 2e^- + H^+$$

The electrons flow to the positive electrode, oxidizing the lead dioxide with sulfuric acid hydrogen ions to form lead sulfate and releasing water.

$$PbO_2 + HSO_4^- + 3H^+ + 2e^- \rightleftharpoons PbSO_4 + 2H_2O$$

The complete oxidation/reduction process is:

$$Pb + PbO_2 + 2HSO_4^- + 2H^+ \rightleftharpoons PbSO_4 + 2H_2O,$$

where the charging process is the symmetric reduction of the lead sulfate in the negative and positive electrodes to lead and lead dioxide, respectively.

Following the laws of fluid dynamics, the sulfuric acid in the separator diffuses outward to the electrodes to equilibrate the imbalance in concentration. To summarize for each cell pair, the discharge process diminishes the concentration of sulfuric acid in both electrodes through oxidation and water release, and in the separator through diffusion. Also, this decrease in sulfuric acid concentration is approximately proportional to the battery utilization, as measured by the amount of lead or lead dioxide ions oxidized to lead sulfate [5, 19].

3.1.4 Previous Research

The first mathematical models developed to describe lead-acid batteries date back to 1958 with Stein [34] and 1961 with Euler [15], and focused on the positive electrode dynamics only. Newman and Tiedemann [29] provide a summary of the numerous contributors who improved these early models. In 1987, White et al [19] further expanded these improvements into a mathematical model describing the five major electrochemical dynamics during a full cycle of discharge, charge, and rest for a complete battery cell pair: acid concentration, electrode porosity, electrolyte current density, electrode potential, and electrolyte (liquid) potential. Temperature and several other variables, whose averaged values were described in detail by Dunning [14] and Trainham [38], were assumed constant. In this model, the five explicit dynamical variables are acid concentration, electrode porosity, electrolyte current density, electrode potential, and electrolyte

potential. Temperature, as well as several other variables whose averaged values were described in detail by Dunning [14] and Trainham [38], are assumed constant. The model developed by White et al [19] consisted of a system of five coupled PDEs, necessary initial and (outer and inner interface) boundary conditions, and intermediary relations. The physical phenomena described by this model are the following:

1. The conversion of active electrode material in the electrochemical reaction.

2. Ohm's law applied to electrolyte and electrode potential.

3. The change in acid concentration due to the diffusion, migration, and depletion of acid caused by the electrochemical reaction in each electrode.

   As an illustration, the governing equation for the acid concentration is

$$\varepsilon \frac{\partial C}{\partial t} = \frac{\partial}{\partial x}\left(D_\varepsilon \frac{\partial C}{\partial x}\right) + K_1 i \frac{\partial C}{\partial x} + (cK_2 + K_3)\frac{\partial i}{\partial x}.$$

4. Kinetic expressions of the electrode reaction according to the Butler-Volmer equation.

The outer boundary conditions represent the assumed symmetry of electrochemical dynamics between each cell pair, whereas the interface conditions represent the continuity of the electrolyte fluid at the material interfaces. These are due to the assumption that the electrodes are homogeneous materials in the macroscopic scale. To solve this system numerically, White et al [19] referred to an implicit time stepping method [30].

This traditional model was modified in 2001 by Tenno et al [37] in developing a quicker, yet accurate computational method. The comparison of this modified model's calculated and measured voltage was remarkably accurate, yet Tenno et al [37] did not

clearly specify how the voltage was calculated from the acid concentration. Some of the major modifications to the traditional model were the combination of the migration and diffusion terms and the introduction of the source of charge variable, which is a proportion of total charge used to calculate the amount of active surface area of each electrode. This modified model has six explicit unknowns: acid concentration, electrode porosity, current density, electrode potential, electrolyte, potential, and source of charge. These unknowns were modeled with a system of six coupled PDEs, the necessary initial and (outer and interface) boundary conditions, and several intermediary relations. For example, the governing equation for acid concentration was:

$$\varepsilon \frac{\partial C}{\partial t} = \frac{\partial}{\partial x}\left(D_{\varepsilon}\frac{\partial C}{\partial x}\right) + (cK_1 + K_2)\frac{\partial i}{\partial x}, \tag{3.1}$$

where the change in current density, $\frac{\partial i}{\partial x}$, is calculated according to the Butler-Volmer equation,

$$\frac{\partial i}{\partial x} = Ai^0\left(\frac{C}{C_{ref}}\right)^{\beta}\exp\left\{\frac{aF\eta}{RT}\right\}\left(1-\exp\left\{\frac{-2F\eta}{RT}\right\}\right).$$

Tenno et al [37] proposed three explicit time step methods, varying in speed and accuracy, to solve their system numerically. A remarkable feature of their numerical solution is the low percentage error in modeling the cell voltage dynamics as compared with measured parameters.

3.2 Development of Sulfuric Acid Model

3.2.1 Conservation of Mass

To develop the diffusion model for the sulfuric acid between electrodes, we begin with the conservation of mass. Since we are considering the mass of sulfuric acid, we can

nondimensionalize this as the conservation of ions. Considering an infinitesimal volume of material inside a battery cell, we have the following relation:

$$\text{Ion change} = \text{Ions in - Ions out} + \text{Ions generated}$$

Taking the limit, this relation leads to the continuity equation,

$$\frac{\partial c}{\partial t} + \nabla \cdot J = s,$$

where c is the molar concentration $\left(\frac{mol}{m^3}\right)$, t is the time in seconds, x is position in meters, $J = J(x)$ is the flux of ions entering the volume at position x in $\frac{mol}{m^2 sec}$, and the source term s expresses the mass generation per volume in $\frac{mol}{m^3 sec}$. From Fick's first law of diffusion [4], the flux of ions past a perpendicular plane is proportional to the concentration gradient across the plane:

$$J = -D\nabla c,$$

where D is the steady-state diffusion coefficient in $\frac{m^2}{sec}$. Since the reaction which consumes sulfuric acid during discharge is driven by the current, or load placed upon the battery, the source term for discharge can be written as

$$s = -\frac{\partial H}{\partial Q}\frac{\partial i}{\partial x},$$

where $\frac{\partial H}{\partial Q}$ is the equivalent molarity to charge ratio with units $\frac{mol}{C}$, and $\frac{\partial i}{\partial x}$ is the spatial change in current density with units $\frac{A}{m^3}$.

Together, the governing diffusion equation for discharge takes the form:

$$\frac{\partial c}{\partial t} = \nabla \cdot D\nabla c - \frac{\partial H}{\partial Q}\frac{\partial i}{\partial x}.$$

3.2.2 Dimensional Reduction

We begin by assuming the manufacture of the battery is uniform, up to a small tolerance. That is, the battery is composed of six uniform battery cell, with each cell containing sixteen uniform negative and fifteen uniform positive electrodes woven together with a homogeneous separator and saturated evenly with acid. It is also reasonable to assume the preformed electrode paste was mixed evenly to create a uniform distribution of lead oxide particles. The separator wrap, charging process, and curing period preserve the macro-homogeneity to create the negative lead and positive lead dioxide electrodes.

Because of this uniformity, and the fact that the current collecting grid interfaces the full cross-section of the the electrode center, any section of the battery cell cut perpendicular to the electrodes will yield the same material properties and thus the same electrochemical dynamics.

Hence, by considering the intersection of any two perpendicular cuts of a battery cell, we can reduce the problem from three dimensions to one. By the uniformity of the negative and positive electrodes, respectively, we can further reduce our analysis to one system of a negative electrode, separator, and positive electrode. Electrodes are constructed by symmetrically pasting a current collecting, nonporous, lead grid. Thus, we can assume the electrochemical dynamics in each electrode are symmetric about the grid.

Therefore our spatial solution region reduces to the one-dimensional interval from the center of the negative electrode (edge of the grid), through the separator, to the center of the positive electrode. See figure (10) for a schematic of this final spatial reduction of the problem. This region of the battery cell is called the cell pair.

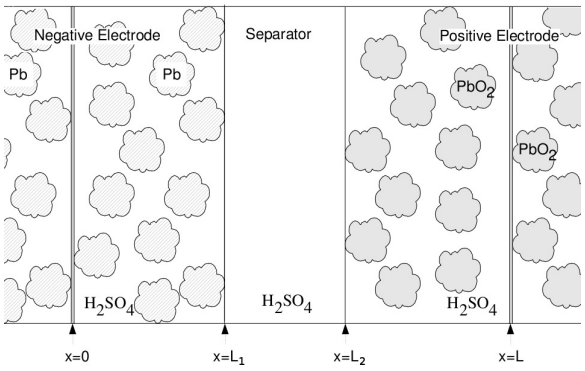

Figure 10: Two-dimensional representation of a fully charged battery cell pair.

In general, a VRLA battery is a combination of battery cells, where each cell is composed of a stack of alternating negative and positive electrodes, separated by a highly porous sheath called the separator, and saturated with sulfuric acid. A pressure sensitive release valve accompanies the outer casing to manage the gases created by the normal reactions. A cell pair consists of half of a negative electrode, one separator layer, and half of a positive electrode, where the current collecting/dissipating grids mark the middle of each electrode [42].

3.2.3 Simplifying Assumptions

Under certain tolerances, each component of the battery is manufactured uniformly, particularly the paste on the preformed electrodes. This means that any cross-section of the battery cell cut perpendicular to the electrodes yields the same material properties, and thus the same electrochemical dynamics. Also, each individual cell pair is mirrored throughout each battery cell. By these symmetries, we reduce the three dimensional problem down to a perpendicular line through an individual cell pair with end points at the lead grids at the centers of the negative and positive electrodes, respectively.

Because of the discontinuities of the material properties and thus parameters within this spatial region $(0, L)$, we decompose it into three disjoint subregions, $\Omega_1 = (0, L_1)$, $\Omega_2 = (L_1, L_2)$, $\Omega_3 = (L_2, L)$, corresponding to the negative electrode half, separator, and the positive electrode half shown in figure (11). Thus, the solution to our PDE lives in the space $(0, L_1) \cup (L_1, L_2) \cup (L_2, L) \times (0, \infty)$.

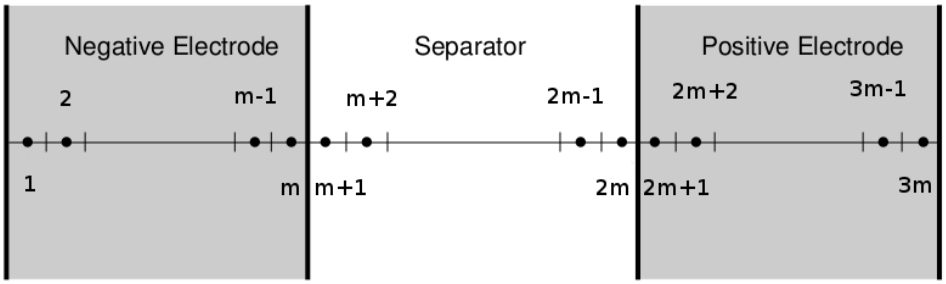

Figure 11: Representation of the one-dimensional cross-section discretization of a battery cell pair.

It is reasonable to assume that acid concentration is a continuous function, since this fluid flows throughout the composite material. To preserve this continuity of solution, we apply matching flux conditions at the interfaces of the material subregions [19]. Combining the governing PDE over the disjoint space with the outer and inner boundary conditions and an initial condition of uniform distribution (to simulate the battery starting at rest), we have the Initial Boundary Valued Problem (IBVP) over $[0, L] \times [0, \infty)$ as described by the following three coupled subproblems.

To simplify and combine Tenno's systems [37] into one partial differential system, we have assumed that temperature, active surface area, and porosity are constant, using average values, and that overpotential can be assumed constant at each step, then solved in a decoupled manner. The following is the justification for these simplifying assumptions.

- The batteries were tested at a controlled temperature between 40 and 48 degrees Celsius. A similar temperature control is reasonable to assume, thus making the temperature variable constant.

- Tenno et al argue that we can assume a constant surface area if "small variation of battery capacity is considered" [37]. Since the batteries we model are relatively newly formed and due to the rechargeable nature of the lead acid battery, we can easily assume that the capacity does not drop much after between one charge-discharge cycle. Treating the surface area as constant is thus admissible, however, it is one of the most difficult battery characteristics to measure, even when assumed constant.

- According to Tenno et al [37], porosity of the electrode varies gradually as the metal expands in a "V"-shaped pattern, differing by 25% at the extremes. Changing porosity from a dynamic to a static variable considerably simplifies the model from a coupled nonlinear system of two PDEs to one nonlinear PDE. Thus, an average value will be used as an approximation.

3.2.4 Sulfuric Acid Model

We develop our model by applying the previous simplifying assumptions to the following reaction-diffusion model [37],

$$\begin{aligned} \varepsilon \frac{\partial c}{\partial t} &= \frac{\partial}{\partial x} D \varepsilon^{\beta} \frac{\partial c}{\partial x} + (cK_1 + K_4) \frac{\partial i}{\partial x}, \\ \text{with } c(x,0) &= c_{\text{ref}}, \qquad x \in \Omega_1,\ t > 0, \end{aligned}$$

with additional relations,

$$\begin{aligned}\frac{\partial \varepsilon}{\partial t} &= K_1 \frac{\partial i}{\partial x}, \\ \frac{\partial i}{\partial x} &= \mathcal{A} i_0 \left(\frac{c}{c_{\text{ref}}}\right)^{\beta} \left(\exp\left\{\frac{\alpha_a F \eta}{RT}\right\} - \exp\left\{\frac{(\alpha_a - 2) F \eta}{RT}\right\}\right),\end{aligned}$$

where ε is the porosity, c and c_{ref} the variable and initial sulfuric acid concentrations, D the diffusion coefficient, β the tortuosity exponent, K_1 the volume to charge ratio, K_4 the molarity to charge ratio, i the current density, α_a is the anodic apparent transfer coefficient, $\mathcal{A}$ the active surface area per volume, i_0 the exchange current density, F Faraday's constant, η the overpotential, R the universal gas constant, and T the temperature. For simplification, we write $c^{ref} \equiv c_{ref}$, $K \equiv K_4$, $i^0 \equiv i_0$, $2\alpha \equiv \alpha_a$, $A^S \equiv \mathcal{A}$, and approximate $\beta = \frac{1}{2}$ to match the morphology of the twistedness of the path for discharge [37]. To simplify and combine the expanded model [37] into an initial boundary value problem, we assume that discharge current, temperature, active surface area, overpotential, and porosity are constants. Consequently, $\frac{\partial \varepsilon}{\partial t} = 0$, so we drop the K_1 portion of the reaction term.

Hence, the IBVP for sulfuric acid concentration in a VRLA battery, under the simplifying assumptions prescribed in subsection 3.2.3, is modeled by the following system of equations and conditions.

First, symmetry and continuity of the concentration are preserved at the current-collecting grid in the center of the negative electrode,

$$\frac{\partial c}{\partial x}(0, t) = 0, \quad t > 0. \tag{3.2}$$

In the relevant half of the negative electrode, charge is released during discharge as the lead (Pb) and sulfuric acid (H_2SO_4) react, diminishing the concentration, to produce

lead sulfate ($PbSO_4$) and release hydrogen gas (H_2) [42]. This consumption and diffusion of sulfuric acid is modeled by the reaction-diffusion equation,

$$\begin{aligned} \frac{\partial c}{\partial t} &= \frac{D}{\sqrt{\varepsilon_1}}\frac{\partial^2 c}{\partial x^2} - b_1\sqrt{c}, \\ c(x,0) &= c^{ref}, \qquad x \in \Omega_1,\ t > 0. \end{aligned} \tag{3.3}$$

At the interface between the negative electrode and separator, the material/chemical parameters change abruptly. To preserve fluidity, the continuity of the concentration is preserved and the flux across the interface is matched by the equations,

$$c(L_1^-, t) = c(L_1^+, t), \tag{3.4}$$

$$D\sqrt{\varepsilon_1}\frac{\partial c}{\partial x}(L_1^-, t) = D\sqrt{\varepsilon_2}\frac{\partial c}{\partial x}(L_1^+, t), \tag{3.5}$$

$$\text{where } L_j^- = \lim_{x \to L_j^-} x, \qquad L_j^+ = \lim_{x \to L_j^+} x, \quad t > 0.$$

Since the material composing the separator mesh is inert with respect to the sulfuric acid, concentration is merely diminished by the fluidic diffusion outward to the two electrodes, as described by the diffusion equation,

$$\begin{aligned} \frac{\partial c}{\partial t} &= \frac{D}{\sqrt{\varepsilon_2}}\frac{\partial^2 c}{\partial x^2}, \\ c(x,0) &= c^{ref}, \qquad x \in \Omega_2,\ t > 0. \end{aligned} \tag{3.6}$$

At the separator-positive electrode interface, the discontinuity of the material parameters are similarly countered by preserving concentration continuity and matching the flux to preserve fluidity:

$$c(L_2^-, t) = c(L_2^+, t), \quad t > 0, \tag{3.7}$$

$$D\sqrt{\varepsilon_2}\frac{\partial c}{\partial x}(L_2^-, t) = D\sqrt{\varepsilon_3}\frac{\partial c}{\partial x}(L_2^+, t), \quad t > 0. \tag{3.8}$$

In the positive electrode half, charge is absorbed during discharge as the lead dioxide (PbO_2) and sulfuric acid react, again diminishing the concentration, to produce lead sulfate and water (H_2O) [42]. This is modeled by

$$\begin{aligned} \frac{\partial c}{\partial t} &= \frac{D}{\sqrt{\varepsilon_3}}\frac{\partial^2 c}{\partial x^2} - b_3\sqrt{c}, \\ c(x,0) &= c^{ref}, \qquad x \in \Omega_3,\ t > 0. \end{aligned} \tag{3.9}$$

Symmetry and continuity of the concentration are also preserved at the grid in the center of the positive electrode by

$$\frac{\partial c}{\partial x}(L,t) = 0, \quad t > 0. \tag{3.10}$$

Note that the coefficients are defined in terms of chemical and material properties of the VRLA battery under discharge. The effective diffusion rate includes the reference diffusion coefficient D, and the porosity ε. The reaction rate coefficient is an expansion of the standard Butler-Volmer equation [19]:

$$\begin{aligned} b_j &= \frac{A_j^S i_j^0 K_j}{\varepsilon_j\sqrt{c^0}}\left(\exp\left\{\frac{2\alpha_j F\eta_j}{RT}\right\} - \exp\left\{\frac{2(\alpha_j - 1)F\eta_j}{RT}\right\}\right), \\ j &= 1, 3, \end{aligned}$$

where $b_2 = 0$ due to the nonreactive separator material, A^S is the active surface area, i^0 the exchange current density, c^0 the reference concentration, α the anodic apparent transfer coefficient, η the surface overpotential, R the universal gas constant, T temperature, and K the equivalent molarity to charge constant, which is defined in the three regions $[\Omega_1, \Omega_2, \Omega_3]$ as

$$K = \left[-\frac{2t_0^+ - 1}{2F},\ 0,\ \frac{2t_0^+ - 3}{2F}\right],$$

where F is Faraday's constant, and t_+ the transference number. Note that each parameter is piecewise constant in relation to the three regions.

To summarize, our simplified sulfuric acid concentration model shown in equations (3.2) – (3.10) in a VRLA battery under the prescribed simplifying assumptions is described by the following coupled PDE system:

$$\begin{cases} \frac{\partial c}{\partial t} = D\varepsilon_1^{\beta-1}\frac{\partial^2 c}{\partial x^2} - b_1 c^\beta, & x \in \Omega_1 = (0, L_1), t > 0, \\ \frac{\partial c}{\partial x}(0,t) = 0, & t > 0, \\ c\,(L_1, t) = \alpha_1, & t > 0, \\ -D\varepsilon_1^{\beta-1}\frac{\partial c}{\partial x}(L_1, t) = \beta_1, & t > 0, \end{cases} \tag{3.11}$$

$$\begin{cases} \frac{\partial c}{\partial t} = D\varepsilon_2^{\beta-1}\frac{\partial^2 c}{\partial x^2}, & x \in \Omega_2 = (L_1, L_2), t > 0, \\ c\,(L_1, t) = \alpha_1, & t > 0, \\ -D\varepsilon_2^{\beta-1}\frac{\partial c}{\partial x}(L_1, t) = \beta_1, & t > 0, \\ c\,(L_2, t) = \alpha_2, & t > 0, \\ -D\varepsilon_2^{\beta-1}\frac{\partial c}{\partial x}(L_2, t) = \beta_2, & t > 0, \end{cases}$$

$$\begin{cases} \frac{\partial c}{\partial t} = D\varepsilon_3^{\beta-1}\frac{\partial^2 c}{\partial x^2} - b_3 c^\beta, & x \in \Omega_3 = (L_2, L), t > 0, \\ c\,(L_2, t) = \alpha_2, & t > 0, \\ -D\varepsilon_3^{\beta-1}\frac{\partial c}{\partial x}(L_2, t) = \beta_2, & t > 0, \\ \frac{\partial c}{\partial x}(L, t) = 0, \end{cases}$$

where

$$b_j = \frac{A_j^S i_j^0 K_j}{c_{ref}^\beta}\left(\exp\left\{\frac{2\alpha_j F\eta_j}{RT}\right\} - \exp\left\{\frac{2(\alpha_j - 1)F\eta_j}{RT}\right\}\right),\ x \in \Omega_j,$$
$$K = \left[-\frac{2t_+^0 - 1}{2F}, 0, \frac{2t_+^0 - 3}{2F}\right],$$
$$\beta = \tfrac{1}{2},$$

and $\alpha_1, \beta_1, \alpha_2, \beta_2$ are coupling values linking the inner boundary conditions.

3.3 Development of Battery Voltage Model

To compare our simulated concentration to the measured voltage we develop a model for lead-acid battery voltage. Battery voltage is a combination of the acid concentration-dependent equilibrium potential and voltage drops caused by cell resistance and generated current. This battery voltage is further modeled as a combination of six battery cells, which are connected in series, to correspond with the design of the batteries tested. Focusing on a battery cell individually, the equilibrium potential is modeled by the Nernst equation [5, 9],

$$U^E = U^0 + \frac{2RT}{F} \ln \left(f c_{\min} \right), \tag{3.12}$$

where U^E is the equilibrium cell potential, U^0 the standard equilibrium cell potential, R the universal gas constant, T temperature, f the activity coefficient of sulfuric acid, and $c_{\min}$ the minimum concentration at each time step.

The Nernst equation is derived from first principles in the following manner. First, since the air above the electrolyte in the battery is an ideal gas [9], the vapor pressure of the electrolyte is

$$P = \frac{nRT}{V}. \tag{3.13}$$

Then, the change in entropy for a general molecule A caused by the reversible movement of one mole ($n = 1$) of A between the electrolyte and the electrode is proportional to the isothermal work of this pressure from the standard to current volume [9]:

$$\begin{aligned} \Delta S_A &= \frac{1}{T} \int_{V^0}^{V} P dV \\ &= \frac{1}{T} \int_{V^0}^{V} \frac{RT}{V} dV \\ &= R \ln \left(\frac{V}{V^0} \right). \end{aligned} \tag{3.14}$$

Since the sulfuric acid solution is not an ideal solution, Raoult's law [9] relates the relative drop in partial vapor pressure, P, from saturation, P^*, of the solute A to its activity, a_A, instead of its concentration (mole fraction), x_A,

$$\begin{aligned} \frac{P^* - P}{P^*} &= 1 - a_A \\ \implies P &= P^* a_A. \end{aligned}$$

Again utilizing the ideal gas law (3.13), we substitute in for the two volumes in the entropy model (3.14) to write it in terms of the ratio of activities,

$$\begin{aligned} \Delta S_A &= R \ln \left(\frac{(K a_A)^{-1}}{(K a_A^0)^{-1}} \right), \quad K = \frac{P^*}{RT}, \\ &= -R \ln \left(\frac{a_A}{a_A^0} \right). \end{aligned} \tag{3.15}$$

Since sulfuric acid has a high dissociation constant [22], we consider the chemical reaction

$$Pb + PbO_2 + 2H^+ + 2HSO_4^- \overset{\text{discharge}}{\rightleftharpoons} PbSO_4 + 2H_2O. \tag{3.16}$$

Since Pb, PbO_2, and $PbSO_4$ are in purely condensed forms, their activities are insignificantly changed from their standard values, so their entropy change is approximately zero. Then, the change in Gibbs free energy is calculated from the activities of the remainder, using the previous entropy model (3.15),

$$\begin{aligned} \Delta G &= \Delta H - T \Delta S_{\text{reaction}} \\ &= \Delta H - T \sum \Delta S_{\text{reaction}} \\ &= \Delta H + RT \left(\sum_{i \in \mathcal{P}} \ln \left(\frac{a_i}{a_i^0} \right) + \sum_{i \in \mathcal{R}} \ln \left(\frac{a_j^0}{a_j} \right) \right) \\ &= \Delta G^0 + RT \left(2 \ln a_{H_2O} - 2 \ln a_{H^+} - 2 \ln a_{HSO_4^-} \right) \\ &= \Delta G^0 + 2RT \ln \frac{a_{H_2O}}{a_{H^+} a_{HSO_4^-}}, \end{aligned}$$

where the standard change in Gibbs free energy, ΔG^0, collects the change in enthalpy, ΔH, as well as the standard entropy values, and $\mathcal{P}$ and $\mathcal{R}$ are the sets of products and reactants, respectively [9].

The lead in the negative electrode releases two electrons, $Pb \rightarrow Pb^{2+} + 2e^-$, before bonding to SO_4^{2-}, which are subsequently absorbed by lead ions in the positive electrode, $Pb^{4+} + 2e^- \rightarrow Pb^{2+}$, before bonding with SO_4^{2-} as well. Thus, the change in Gibb's free energy of the chemical reaction is balanced by the electrical work at the equilibrium cell potential, U,

$$\Delta G = -nFU, \quad \text{where } n = 2.$$

Through substitution, the equilibrium cell potential can be written in terms of the activities. Since the solution is largely water, we assume $a_{H_2O} = 1$ [5]. Further, since we have assumed the sulfuric acid dissociates evenly into H^+ and HSO_4^-, then their concentrations are approximately equal, and so are their activities: $a_{H_2SO_4} = a_{H^+} = a_{HSO_4^-}$ [5]. Further, activity can be written as an activity coefficient, f, times the concentration, where the minimum concentration is taken to determine the equilibrium voltage. Thus, the equilibrium cell potential becomes the Nernst equation (3.12),

$$\begin{aligned} U &= -\frac{\Delta G}{2F} \\ &= -\frac{\Delta G^0}{2F} - \frac{RT}{F} \ln \frac{a_{H_2O}}{a_{H^+} a_{HSO_4^-}} \\ &= -\frac{\Delta G^0}{2F} - \frac{RT}{F} \ln \frac{1}{a_{H_2SO_4}^2} \\ &= U^0 + \frac{2RT}{F} \ln(f c_{\min}) \end{aligned}$$

Since the test batteries are a combination of six battery cells connected in series, this equilibrium voltage (3.12) is multiplied by six to calculate the equilibrium voltage of the

entire battery.

In sum, by our simplifying assumptions, the Nernst equation has been derived from first principles using the ideal gas law to quantify the vapor pressure above the solution, Raoult's law to relate to the activity of this non-ideal liquid, reversible isothermal work to transfer electrolyte ions across the interfaces, and finally we obtained the equilibrium voltage through the change in Gibb's free energy of the chemical reaction (3.16). Thus, using the Nernst equation to model this equilibrium potential combined with voltage drops associate with the generated current and cell resistance, the battery voltage is computed for six battery cells in series,

$$\begin{aligned} V =& 6\left(U^E - \eta_3 + \eta_1 - N^{\text{cell}} i^{\text{cell}} r\right) \\ =& 6\left(\left(\left(U_3^0 - \eta_3\right) - \left(U_1^0 - \eta_1\right)\right) + \frac{RT}{F}\ln\left(f c_{\min}\right) - N^{\text{cell}} i^{\text{cell}} r\right), \end{aligned} \tag{3.17}$$

where U_1^0, U_3^0 are the two half-electrode potentials, η_1, η_3 the two overpotentials reducing their respective electrode potentials, f the mean molar activity coefficient, $c_{\min}$ the minimum concentration at that time step, N^{cell} is the number of cell-pairs in a cell, i^{cell} is the current in each cell-pair, and r is the bulk cell resistance.

3.4 Numerical Solution

3.4.1 Operator Splitting Implementation

Due to the complications caused by the parameter discontinuities and the nonlinearity of the problem, we implement an operator splitting method with 'NL' recombination scheme from section 1.1.4 to solve the governing system (3.11). The general form of the

governing equations (3.11),

$$\frac{\partial c}{\partial t} = \frac{D_j}{\sqrt{\varepsilon_j}} \frac{\partial^2 c}{\partial x^2} - b_j \sqrt{c}, \quad x_j \in \Omega_j, t > 0,$$

is split into a reaction step,

$$\frac{\partial c}{\partial t} = -b_j \sqrt{c}, \quad x_j \in \Omega_j, t > 0 \tag{3.18}$$

which happens to be spatially independent, and a diffusion step,

$$\frac{\partial c}{\partial t} = \frac{D_j}{\sqrt{\varepsilon_j}} \frac{\partial^2 c}{\partial x^2} \quad x_j \in \Omega_j, t > 0, \tag{3.19}$$

which is linear. Simplified as such, we solve the reaction step exactly,

$$r(c_i^n, \Delta t) = \left[-\frac{b\Delta t}{2} + \sqrt{c_i^n} \right]^2,$$

and solve the diffusion step with the backward Euler solution,

$$Bc^{n+1} = c^n, \tag{3.20}$$

where the approximation matrix B is constructed in section 3.4.2.

The operator is split by solving a reaction step (3.18) from time index n to $n + 1/2$ and then a diffusion step (3.19) from $n + 1/2$ to $n + 1$. As proven in section 1.1.4, this type of splitting is first order accurate in time. Further, as the split solutions are solved using an exact solution and an unconditionally stable backward Euler numerical solution, which is also unconditionally oscillation-free, section 2.2.4.2 proves that the operator splitting solution as a whole is unconditionally stable.

3.4.2 Discretization

Due to discontinuous parameter jumps at composite media boundaries, special care must be taken in discretizing the spatial region. In response to these discontinuities, each subregion is discretized disjointly so that the one-dimensional cell pair is discretized into m

nodes with $m = m_1 + m_2 + m_3$, each node centered in an interval so as to avoid computing the concentration at the electrode−separator interfaces. Accordingly, the spatial derivatives of the model (3.2-3.10) are approximated in each subregion independently up to the boundaries using one-sided schemes and ghost points. The subregions are then coupled through the substitutions of the boundary conditions at the interfaces. Refer to figure 12 for a diagram of this discretization.

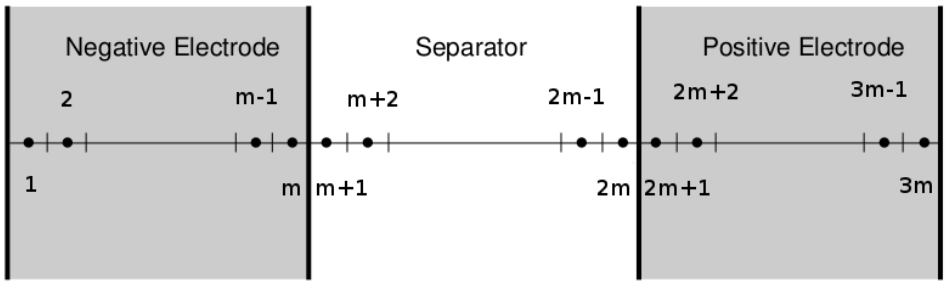

Figure 12: Discretization of one-dimensional reduction of a battery cell pair. Note that the nodes m and $2m$ precede their respective interfaces.

We choose the backward Euler method as our temporal scheme to maintain stability without restriction to step size in time. Although this simple method is only first order accurate, this level of accuracy matches the order of the time derivative. Using a higher order differencing in time could create extraneous solutions [6].

$$\frac{\partial}{\partial t} c_i^{n+1} = \frac{c_i^{n+1} - c_i^n}{\Delta t} + O(\Delta t).$$

Due to our choice of the backward Euler scheme, all of our spatial approximations will be at the $n+1$ time step. For all nodes not neighboring the material interfaces, the diffusion equation is approximated as follows:

$$\frac{\partial}{\partial t} c_i^{n+1} - \frac{D}{\sqrt{\varepsilon}} \frac{\partial^2}{\partial x^2} c_i^{n+1} = \frac{c_i^{n+1} - c_i^n}{\Delta t} - \frac{D}{\sqrt{\varepsilon}} \frac{c_{i-1}^{n+1} - 2c_i^{n+1} + c_{i+1}^{n+1}}{\Delta x^2} + O\left(\Delta t + \Delta x^2\right), \quad (3.21)$$

for $i \neq m, m+1, 2m, 2m+1$, while we develop left and right one-sided schemes for the second derivative centered on the nodes neighboring the material interfaces. Note, equation (3.21) does hold for the nodes neighboring the outer boundary since we use symmetric ghost point approximations on the boundary conditions. We develop the left one-sided scheme using the method of undetermined coefficients, beginning with a scheme of the form

$$\frac{\partial^2}{\partial x^2} c_i^{n+1} = \frac{1}{\Delta x^2} \left[k_{-2} c_{i-2}^{n+1} + k_{-1} c_{i-1}^{n+1} + k_0 c_i^{n+1} + k_{1/2} c_{i+1/2}^{n+1} + O\left(\Delta x^4\right) \right],$$

for $i = m, 2m,\ k_{1/2} \neq 0$, which we desire to be second order accurate. The $k_{1/2} \neq 0$ restriction is critical since the interface half-nodes must contribute to our governing equations before we can use the flux preservation conditions (3.11) to substitute them out of the approximation equations.

Using Taylor expansions, we expand as

$$\begin{aligned} \tfrac{\partial^2}{\partial x^2} c_i^{n+1} \;=\; & \tfrac{1}{\Delta x^2} \left[(k_{-2} + k_{-1} + k_0 + k_{1/2}) c_i^{n+1} + \left(-2k_{-2} - k_{-1} + \tfrac{1}{2} k_{1/2}\right) \Delta x \tfrac{\partial}{\partial x} c_i^{n+1} \right. \\ & + \left(2k_{-2} + \tfrac{1}{2} k_{-1} + \tfrac{1}{8} k_{1/2}\right) \Delta x^2 \tfrac{\partial^2}{\partial x^2} c_i^{n+1} \\ & \left. + \left(-\tfrac{4}{3} k_{-2} - \tfrac{1}{6} k_{-1} + \tfrac{1}{48} k_{1/2}\right) \Delta x^3 \tfrac{\partial^3}{\partial x^3} c_i^{n+1} + O\left(\Delta x^4\right) \right] \end{aligned}$$

and then solve the linear system,

$$\left[\begin{array}{cccc|c} 1 & 1 & 1 & 1 & 0 \\ -2 & -1 & 0 & 1/2 & 0 \\ 2 & 1/2 & 0 & 1/8 & 1 \\ -4/3 & -1/6 & 0 & 1/48 & 0 \end{array}\right] \quad \Longrightarrow \quad \left[\begin{array}{cccc|c} 1 & 0 & 0 & 0 & -1/5 \\ 0 & 1 & 0 & 0 & 2 \\ 0 & 0 & 1 & 0 & -5 \\ 0 & 0 & 0 & 1 & 1/5 \end{array}\right],$$

to obtain the left one-sided scheme,

$$\frac{\partial^2 c_i^{n+1}}{\partial x^2} = \frac{-\frac{1}{5} c_{i-2}^{n+1} + 2c_{i-1}^{n+1} - 5c_i^{n+1} + \frac{16}{5} c_{i+1/2}^{n+1}}{\Delta x^2} + O\left(\Delta x^2\right),\ i = m, 2m, \tag{3.22}$$

The right one-sided scheme is also developed using the method of undetermined coefficients in a similar fashion to obtain

$$\frac{\partial^2 c_{i+1}^{n+1}}{\partial x^2} = \frac{\frac{16}{5}c_{i+1/2}^{n+1} - 5c_{i+1}^{n+1} + +2c_{i+2}^{n+1} - \frac{1}{5}c_{i+3}^{n+1}}{\Delta x^2} + O\left(\Delta x^2\right), i = m, 2m. \tag{3.23}$$

3.4.3 Boundary and Interface Approximations

At the outer boundaries we will use the ghost point method [6] on the centered difference,

$$\frac{\partial C_{i+1/2}^{n+1}}{\partial x} = \frac{C_{i+1}^{n+1} - C_i^{n+1}}{\Delta x} + O\left(\Delta x^2\right), \ i = 0, m, \tag{3.24}$$

because it matches easily with the Neumann conditions (3.11) and it preserves second order spatial accuracy. Note that because all nodes are centered inside each interval, the 0-node and the 1-node are actually centered about the boundary of the negative electrode grid. This is similar for the $3m$ and $3m+1$-nodes neighboring the positive grid. The centered approximations for the homogeneous Neumann conditions at the outer boundaries (representing the centers of the electrodes) reduce to the substitutions for these fictitious boundary nodes,

$$\begin{aligned} c_0^{n+1} &= c_1^{n+1} + O\left(\Delta x^2\right), \\ c_{m+1}^{n+1} &= c_m^{n+1} + O\left(\Delta x^2\right). \end{aligned} \tag{3.25}$$

At the interfaces we develop left and right one-sided schemes for the first derivative in order to equate the flux from both sides of each material interface. We develop the left one-sided scheme by the method of undetermined coefficients of the following form

$$\frac{\partial}{\partial x} c_{i+1/2^-}^{n+1} = \frac{1}{\Delta x}\left[k_{-3/2}c_{i-1}^{n+1} + k_{-1/2}c_i^{n+1} + k_0 c_{i+1/2}^{n+1}\right], \quad i = m, 2m, \ k_0 \neq 0.$$

Using Taylor expansions, we expand the terms,

$$\begin{aligned}\tfrac{\partial}{\partial x}c^{n+1}_{i+1/2^-} &= \tfrac{1}{\Delta x}\Big[(k_{-3/2}+k_{-1/2}+k_0)c^{n+1}_{i+1/2^-} + \left(-\tfrac{3}{2}k_{-3/2}-\tfrac{1}{2}k_{-1/2}\right)\Delta x\tfrac{\partial}{\partial x}c^{n+1}_{i+1/2^-} \\ &\quad + \left(\tfrac{9}{8}k_{-3/2}+\tfrac{1}{8}k_{-1/2}\right)\Delta x^2\tfrac{\partial^2}{\partial x^2}c^{n+1}_{i+1/2^-} + o(\Delta x^3)\Big],\end{aligned}$$

and solve the following linear system:

$$\left[\begin{array}{ccc|c} 1 & 1 & 1 & 0 \\ -3/2 & -1/2 & 0 & 1 \\ 9/8 & 1/8 & 0 & 0 \end{array}\right] \implies \left[\begin{array}{ccc|c} 1 & 0 & 0 & 1/3 \\ 0 & 1 & 0 & -3 \\ 0 & 0 & 1 & 8/3 \end{array}\right],$$

to obtain the left one-sided scheme,

$$\frac{\partial}{\partial x}c^{n+1}_{i+1/2^-} = \frac{1}{\Delta x}\left[\frac{1}{3}c^{n+1}_{i-1} - 3c^{n+1}_i + \frac{8}{3}c^{n+1}_{i+1/2}\right],\ i = m, 2m. \tag{3.26}$$

The right one-sided scheme is also derived using the method of undetermined coefficients in a similar manner to obtain

$$\frac{\partial c_{i+1/2^+}}{\partial x} = \frac{-\frac{8}{3}c_{i+1/2} + 3c_{i+1} - \frac{1}{3}c_{i+2}}{\Delta x} + o(\Delta x^2), i = m, 2m. \tag{3.27}$$

Then, we substitute these approximations (3.26,3.27) into our flux preservation equations (3.11) at the two interfaces,

$$\begin{aligned} -D\varepsilon_1^{\beta-1}\frac{\partial c_{m+1/2^-}}{\partial x} &= -D\varepsilon_2^{\beta-1}\frac{\partial c_{m+1/2^+}}{\partial x}, \\ -D\varepsilon_2^{\beta-1}\frac{\partial c_{2m+1/2^-}}{\partial x} &= -D\varepsilon_3^{\beta-1}\frac{\partial c_{2m+1/2^+}}{\partial x}, \end{aligned}$$

and solve for the interface half-nodes,

$$\begin{aligned} c^{n+1}_{m+1/2} &= -\tfrac{\delta_{12}}{8}c^{n+1}_{m-1} + \tfrac{9\delta_{12}}{8}c^{n+1}_m + \tfrac{9\delta_{21}}{8}c^{n+1}_{m+1} - \tfrac{\delta_{21}}{8}c^{n+1}_{m+2}, \\ c^{n+1}_{2m+1/2} &= -\tfrac{\delta_{23}}{8}c^{n+1}_{2m-1} + \tfrac{9\delta_{23}}{8}C^{n+1}_{2m} + \tfrac{9\delta_{32}}{8}c^{n+1}_{2m+1} - \tfrac{\delta_{32}}{8}c^{n+1}_{2m+2}, \end{aligned} \tag{3.28}$$

where the simplifying variables $\delta_{12}, \delta_{21}, \delta_{23}, \delta_{32}$ are defined by

$$\delta_{jk} = \frac{\Delta x_k \sqrt{\varepsilon_k}}{\Delta x_j \sqrt{\varepsilon_j} + \Delta x_k \sqrt{\varepsilon_k}}.$$

We then substitute these equations (3.28) back into our one-sided second derivative approximations (3.26,3.27) to result in a set of approximation equations for the nodes neighboring the interfaces. Hence, we approximate our governing equation using these half nodes, though we can not use them in our solution, and then we substitute them out by using the neighboring nodes to preserve the continuity of flow between the materials.

We also develop second order, one-sided schemes to approximate the flux preserving conditions. As an example, equation (3.29) demonstrates the left one-sided scheme at the negative electrode and separator interface,

$$\frac{\partial}{\partial x} c^{n+1}_{m+1/2^-} = \frac{1}{\Delta x}\left[\frac{1}{3} c^{n+1}_{m-1} - 3c^{n+1}_{m} + \frac{8}{3} c^{n+1}_{m+1/2}\right] + O\left(\Delta x^2\right). \tag{3.29}$$

Interface conditions on each side are matched to remove dependence on the interface 'nodes', such as $c_{m+1/2}$ in the previous example.

Seeking the system of equations which define the diffusion split problem across the discretized composite material, we substitute equations $(3.22) - (3.29)$ into the diffusion equation (3.21). Using the simplifying variable

$$\lambda_j \;=\; \frac{D\Delta t}{\sqrt{\varepsilon_j}\Delta x^2},$$

we obtain the following set of approximation equations for the diffusion across the discretized composite material:

$$
\begin{aligned}
&\left.\begin{aligned}
c_1^n &= (1+\lambda_1)\, c_1^{n+1} - \lambda_1 c_2^{n+1} \\
&\qquad\qquad \boxed{i = 2 : m-1} \\
c_i^n &= -\lambda_1 c_{i-1}^{n+1} + (1+2\lambda_1)\, c_i^{n+1} - \lambda_1 c_{i+1}^{n+1}, \\
c_m^n &= \frac{\lambda_1}{5} c_{m-2}^{n+1} - \left(2 - \frac{2\delta_{12}}{5}\right)\lambda_1 c_{m-1}^{n+1} + \left(1 + \left(5 - \frac{18\delta_{12}}{5}\right)\lambda_1\right) c_m^{n+1} \\
&\quad - \frac{18\delta_{21}\lambda_1}{5} c_{m+1}^{n+1} + \frac{2\delta_{21}\lambda_1}{5} c_{m+2}^{n+1}
\end{aligned}\right\} - \\
&\left.\begin{aligned}
c_{m+1}^n &= \frac{2\delta_{12}\lambda_2}{5} c_{m-1}^{n+1} - \frac{18\delta_{12}\lambda_2}{5} c_m^{n+1} + \left(1 + \left(5 - \frac{18\delta_{21}}{5}\right)\lambda_2\right) c_{m+1}^{n+1} \\
&\quad - \left(2 - \frac{2\delta_{21}}{5}\right)\lambda_2 c_{m+2}^{n+1} + \frac{\lambda_2}{5} c_{m+3}^{n+1} \\
&\qquad\qquad \boxed{i = m+2 : 2m-1} \\
c_i^n &= -\lambda_2 c_{i-1}^{n+1} + (1+2\lambda_2)\, c_i^{n+1} - \lambda_2 c_{i+1}^{n+1}, \\
c_{2m}^n &= \frac{\lambda_2}{5} c_{2m-2}^{n+1} - \left(2 - \frac{2\delta_{23}}{5}\right)\lambda_2 c_{2m-1}^{n+1} + \left(1 + \left(5 - \frac{18\delta_{23}}{5}\right)\lambda_2\right) c_{2m}^{n+1} \\
&\quad - \frac{18\delta_{32}\lambda_2}{5} c_{2m+1}^{n+1} + \frac{2\delta_{32}\lambda_2}{5} c_{2m+2}^{n+1}
\end{aligned}\right\} \text{SEP} \\
&\left.\begin{aligned}
c_{2m+1}^n &= \frac{2\delta_{23}\lambda_3}{5} c_{2m-1}^{n+1} - \frac{18\delta_{23}\lambda_3}{5} c_{2m}^{n+1} + \left(1 + \left(5 - \frac{18\delta_{32}}{5}\right)\lambda_3\right) c_{2m+1}^{n+1} \\
&\quad - \left(2 - \frac{2\delta_{32}}{5}\right)\lambda_3 c_{2m+2}^{n+1} + \frac{\lambda_3}{5} c_{2m+3}^{n+1} \\
&\qquad\qquad \boxed{i = 2m+2 : 3m-1} \\
c_i^n &= -\lambda_3 c_{i-1}^{n+1} + (1+2\lambda_3)\, c_i^{n+1} - \lambda_2 c_{i+1}^{n+1}, \\
c_{3m}^n &= -\lambda_3 c_{3m-1}^{n+1} + (1+\lambda_3)\, c_{3m}^{n+1}
\end{aligned}\right\} +
\end{aligned}
\tag{3.30}
$$

These equations (3.30) represent the system $Bc^{n+1} = c^n$, rewritten as $c^n = Bc^{n+1}$ (3.20) for readability, where the $3m \times 3m$ approximation matrix B for the diffusion step is pentadiagonal, and $m = L/(\Delta x_1 + \Delta x_2 + \Delta x_3)$. Notice, however, that B has only four rows containing five nonzero entries; the rest have three which is standard to a

tridiagonal matrix.

3.4.4 Verification of Accuracy and Stability

Since the sulfuric acid reaction-diffusion model is a semilinear parabolic PDE with infinitely differentiable operators, the 'NL' split recombination scheme provides an $O(\Delta t)$ accuracy for the operator splitting, as proven in section 1.1.4. Additionally, the spatial diffusion and boundary conditions were discretized with $O(\Delta x^2)$ accuracy, the reaction split solution was solved exactly, and the diffusion split solution was solved numerical with $O(\Delta t)$ accuracy. Thus, the combined accuracy of the numerical solution to the sulfuric acid reaction-diffusion model is first order in time and second order in space.

Since these split solutions are iterated sequentially, stability of the splitting method depends solely on the stability of it's split solutions [35]. The reaction step is solved exactly, and is hence unconditionally stable. The diffusion step is solved implicitly by the backward Euler method and is thus unconditionally stable. Further, since the backward Euler method has an exponential time factor bounded between zero and one, it is also unconditionally oscillation-free, as shown by Von Neumann analysis in section 2.2.4.2. Hence, the entire numerical solution of the sulfuric acid reaction-diffusion model 3.2 is unconditional stable.

3.5 Results

3.5.1 Parameters

In 2006, batteries designed by CISR were manufactured and tested at an outside company to conduct discharge tests for measuring voltage. These batteries were composed of six cells, and each cell had 13 negative electrodes and 12 positive electrodes. In table 3, parameters $c^{ref}, i^{\text{app}}, L, T, \eta$ are calculated from measurements taken before testing; $A, i^0, t_0^+, \varepsilon, D, f$ are taken from literature [5, 9, 19, 37].

Table 3: Parameter Values used in Numerical Solution: [−, SEP, +]

Symbol	Negative	Separator	Positive	Units [Source]
A	74.2	–	74.2	cm^2 [32]
A^S	237	0	2070	m^2/m^3 [37]
c^{ref}	5.65	5.65	5.65	mol/L [32]
D	4.08×10^{-9}	4.08×10^{-9}	4.08×10^{-9}	m^2/s [19]
f	0.198	0.198	0.198	mol/L [9]
i^{batt}	27	–	27	A [32]
i^0	104	–	6.66	A/m^2 [37]
L	0.546	1.40	0.546	mm [32]
r	0.025	0.025	0.025	Ω [9]
T	311	311	311	K [32]
t_0^+	0.72	–	0.72	– [37]
U^0	-0.336	–	1.79	V [9]
α	0.775	–	0.575	– [37]
ϵ	0.5	0.9	0.45	– [37]

Figure 13 shows the numerical solution of the sulfuric acid concentration model (3.11) under discharge with the parameter values listed in table 3. In comparison to

a fully implicit whole method, our operator splitting solution resulted in remarkable speed-up, as demonstrated in figure 15 and table 4. For an initial mesh size of 15 nodes, table 4 describes the quick run-time per one hour simulated, then the speed-up with this operator splitting solution compared to a fully implicit solution of the whole system, and then the 'acceleration' factor of how the speed-up grows, as this mesh is exponentially refined by factors of 2. Given a sulfuric acid concentration solution profile, the battery voltage model (3.17) computes the simulated voltage. Figure 14 demonstrates the accuracy of this simulated voltage in comparison to the measured voltage curve from a first discharge test at 27 Amps. Though the closeness of our simulation to the data is incredible, this data represents measurement of only one battery. Subsection 3.5.2.3, demonstrates the high variability in the various first-discharge tests done on several batteries manufactured to the same design specifications.

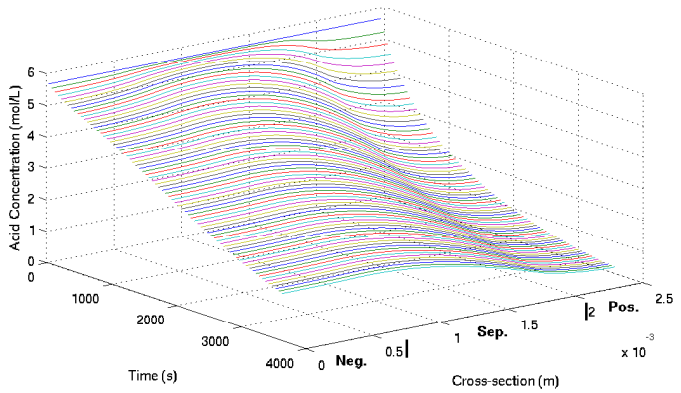

Figure 13: Numerical solution for acid concentration of model (3.2-3.10) during discharge at 27 Amp

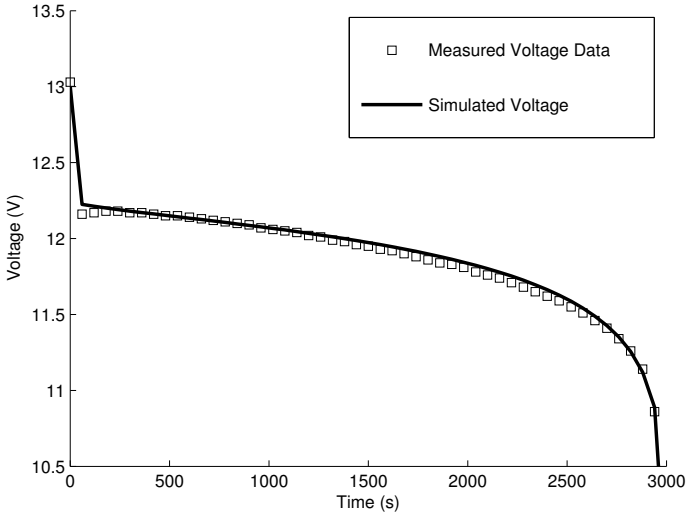

Figure 14: Comparison of simulated and measured battery voltage at 27 Amps.

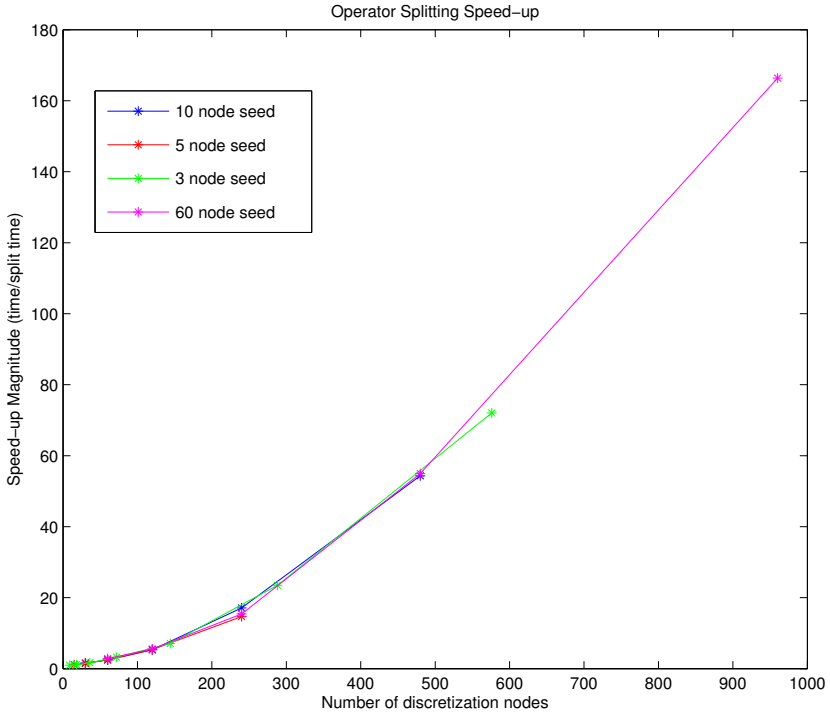

Figure 15: Computational speed-up of operator splitting using four different initial node seeds.

Table 4: Computational Run-time and Speed-Up of Operator Splitting

Number of Total Nodes	Run-time (seconds)	Speed-Up Factor	Speed-Up Acceleration
15	1.15	1.10x	–
30	1.46	1.38x	1.26
60	2.03	2.38x	1.73
120	3.15	5.26x	2.21
240	5.45	16.66x	3.16
480	9.96	53.93x	3.24

3.5.2 Model Calibration

All the electro-chemical constants used that are common to VRLA batteries are taken from the literature [5, 19, 37]. Of the remaining parameter values particular to the batteries' specific formation, several were measured from the test batteries before discharge, but a few internal parameters were immeasurable. These required some calibration of the model and are discussed in subsections 3.5.2.1 and 3.5.2.2. Additionally, the model was further calibrated to deal with variation in the measured voltage data.

3.5.2.1 Overpotential Approximation via Optimization

Unlike other calculated parameters, the overpotential, η, is defined by the following differential inverse problem,

$$\left(\frac{\partial i}{\partial x}\right)_{m_j} = i_j^0 A_j^S \sqrt{\frac{c_{m_j}}{c_{ref}}} \left(\exp\left\{\frac{2\alpha_j F \eta_{m_j}}{RT}\right\} - \exp\left\{\frac{2(\alpha_j - 1) F \eta_{m_j}}{RT}\right\} \right),$$

with current density $i = 0$ at the separator, and $i = i_{\text{app}}$ at the outer boundaries; all parameters are piecewise continuous with respect to each region j and computed for node m_j. Physically, these systems represent the current in the electrolyte solution being equal to the applied current in the separator and diminishing through the electrodes to zero at the grids where the current is collected from the solid electrode matrix. We can

solve this problem for the overpotential at each node in the two electrodes, η_{m_1} and η_{m_3}, using the Newton root finding method [31],

$$\eta_m^{(k+1)} = \eta_m^{(k)} - \frac{E_m\left(\eta_m^{(k)}\right)}{\frac{\partial}{\partial\eta}E_m\left(\eta_m^{(k)}\right)}, \quad \text{node } m = m_j \text{ in electrode } j = 1, 3$$

bound between $-1V$ and $1V$, where these iterative methods start with some initial guess, converge linearly to the nodal overpotentials, and stop when $\left|\eta_m^{(k+1)} - \eta_m^{(k)}\right| < \text{tol}_j$ for some small tolerance (tol_j). The error functions, $E_{m_j}\left(\eta_{m_j}^{(k)}\right)$, are defined for each electrode as

$$\begin{aligned} E_{m_1}(\eta_{m_1}) &= \left(\frac{\partial i}{\partial x}\right)_{m_1} L_1 - i^{\text{app}}, \\ E_{m_3}(\eta_{m_3}) &= \left(\frac{\partial i}{\partial x}\right)_{m_3} L_3 + i^{\text{app}}, \end{aligned}$$

and are computed by integrating over the three subregions individually,

$$\begin{aligned} i_{\text{app}} - 0 &= L_1 i_1^0 A_1^S \sqrt{\frac{c_{m_1}}{c_{ref}}} \left(\exp\left\{\frac{2\alpha_1 F\eta_{m_1}}{RT}\right\} - \exp\left\{\frac{2(\alpha_1 - 1)F\eta_{m_1}}{RT}\right\}\right), \\ i_{\text{app}} - i_{\text{app}} &= 0, \\ 0 - i_{\text{app}} &= L_3 i_3^0 A_3^S \sqrt{\frac{c_{m_3}}{c_{ref}}} \left(\exp\left\{\frac{2\alpha_3 F\eta_{m_3}}{RT}\right\} - \exp\left\{\frac{2(\alpha_3 - 1)F\eta_{m_3}}{RT}\right\}\right), \end{aligned}$$

Due to the difference of exponentials, these error functions have a nearly flat plateau region, as shown in figure 16, and their second derivatives (Hessians) change sign. As the Hessians are globally indefinite, standard nonlinear optimization methods fail, so we solve these two similar minimization problems using a bounded Newton Root finding method applied to the error functions. Starting with some initial guess, the method calculates subsequent iterations based on the recursion,

$$\eta_m^{(k+1)} = \eta_m^{(k)} - \frac{E_m(\eta_m^{(k)})}{\frac{\partial}{\partial\eta}E_m(\eta_m^{(k)})}, \quad \text{node } m = m_j \text{ in electrode } j = 1, 3.$$

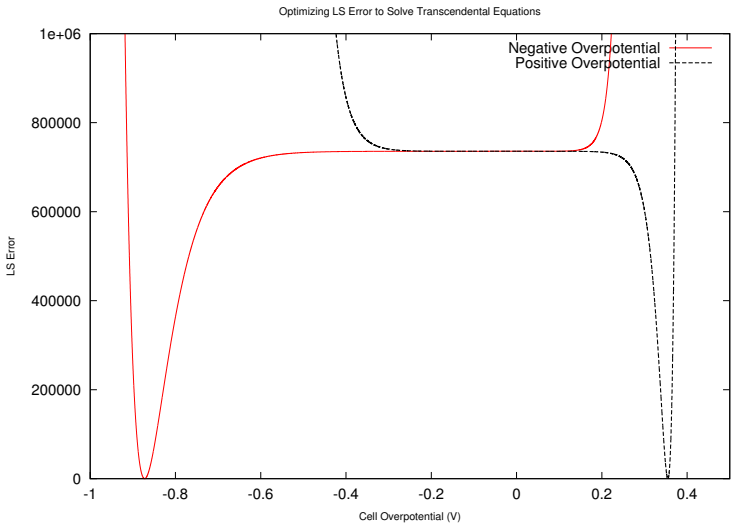

Figure 16: Error functions with plateau regions for overpotential optimization problem.

3.5.2.2 Overpotential via Sinh Approximation

If our anodic and cathodic transfer coefficients, $\alpha_j, (1-\alpha_j)$, are the same value, say for $\alpha_j = .5$, then we can write the solutions,

$$\begin{aligned} i_{\text{app}} - 0 &= L_1 i_1^0 A_1^S \sqrt{\frac{c_{m_1}}{c_{ref}}} \left(\exp\left\{ \frac{F\eta_{m_1}}{RT} \right\} - \exp\left\{ \frac{-F\eta_{m_1}}{RT} \right\} \right), \\ i_{\text{app}} - i_{\text{app}} &= 0, \\ 0 - i_{\text{app}} &= L_3 i_3^0 A_3^S \sqrt{\frac{c_{m_3}}{c_{ref}}} \left(\exp\left\{ \frac{F\eta_{m_3}}{RT} \right\} - \exp\left\{ \frac{-F\eta_{m_3}}{RT} \right\} \right), \end{aligned}$$

to our differential equation in terms of hyperbolic sines

$$\begin{aligned} i_{\text{app}} &= 2L_1 i_1^0 A_1^S \sqrt{\frac{c_{m_1}}{c_{ref}}} \sinh\left(\frac{F\eta_{m_1}}{RT} \right), \\ 0 &= 0, \\ -i_{\text{app}} &= 2L_3 i_3^0 A_3^S \sqrt{\frac{c_{m_3}}{c_{ref}}} \sinh\left(\frac{F\eta_{m_3}}{RT} \right), \end{aligned}$$

which allows us to solve for our nodal overpotentials by direct inversion,

$$\begin{aligned}\eta_{m_1} &= \tfrac{RT}{F} \quad \sinh^{-1}\left(\frac{i_{\text{app}}\sqrt{c_{ref}}}{2L_1 i_1^0 A_1^S \sqrt{c_{m_1}}}\right), \\ \eta_{m_3} &= \tfrac{RT}{F} \quad \sinh^{-1}\left(\frac{-i_{\text{app}}\sqrt{c_{ref}}}{2L_3 i_3^0 A_3^S \sqrt{c_{m_3}}}\right),\end{aligned}$$

where the inverse of the hyperbolic sine is defined as

$$\sinh^{-1}(x) = \ln\left(x + \sqrt{x^2+1}\right).$$

This solution technique for the overpotential is much quicker than the root finding method of section 3.5.2.1, but has an additional assumption on α. Since the anodic transfer coefficient given for the positive electrode in table 3, $\alpha_3 = .575$, is close to .5, this hyperbolic sine approximation is appropriate.

3.5.2.3 Data Variability

AeroVironment, a company in California, USA which specializes in efficient energy systems, conducted 27 Amp discharge tests on batteries designed by CISR. Figure 17 demonstrates the variability between the various first discharge tests of 31 batteries constructed to the same prescribed design. Matching the simulation results to this most recently acquired battery data requires further information about the variability. This is especially evidenced by the 24 minute (of a one hour discharge) spread in drop-off times of the measured voltage. Accordingly, section 3.5 demonstrates in figure 19 how this variability can be accounted for by incomplete charge formation, and that the simulation

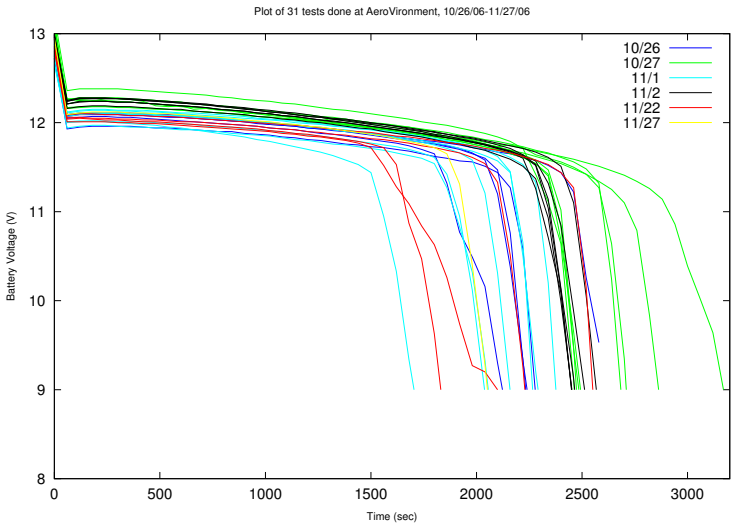

Figure 17: Voltage measurements of first discharge tests for 31 uniformly designed batteries.

can match the spread of discharge curves for batteries tested recently by lowering the maximum allowable utilization to accommodate for this variation in percent formation.

Data collected for one batch of discharges is presented as a whole in Figure 18 to demonstrate data variability in comparison to the simulated voltage, and in part in Figure 19 as the best and worst (discharge life) batteries are compared against the simulated data and one calibrated to account for this variability.

Matching the simulation results to each data strand requires further information about the variability in the data. The batteries tested were newly formed and had not yet been cycled up for uniform fullness of charge; each battery was only discharged once [32]. We assume the only difference between the discharges is fullness of charge represented by the critical volume fraction, u_j^{CVF}, which is the maximum allowable utilization for electrode $j = 1, 3$.

Due to conductive pathway constraints, nodes cannot be utilized beyond a critical

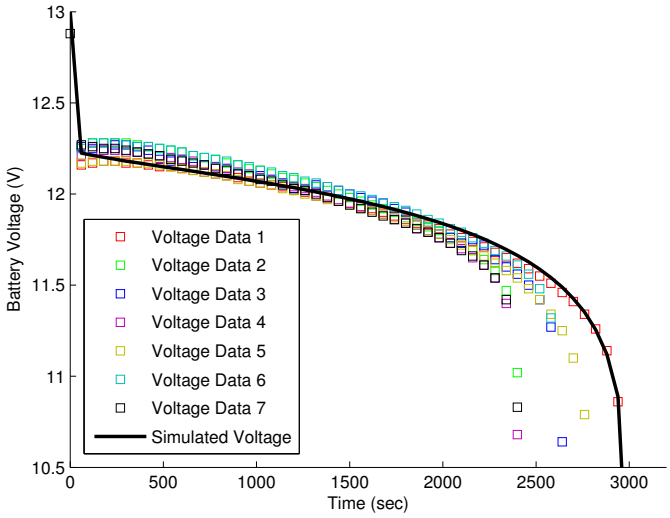

Figure 18: Comparison of simulated voltage against one batch of measured battery voltages from a first-discharge test at 27 Ampheres.

volume fraction, which has been experimentally approximated to be 55% in the positive electrode and 60% in the negative electrode [42]. Since this is more limiting in the positive electrode, we focus our calibration on the maximum allowable utilization for those nodes. Cells not fully charged, however, have less capacity and thus a lower maximum allowable utilization than the electrodes' critical volume fraction. When a nodes' utilization reaches this maximum allowable utilization, that node is shut off, shifting the weight of the discharge to neighboring nodes. The utilization at each node, u, is summed over time as,

$$u = \sum \frac{\Delta V_j \Delta c}{\kappa_j W_j K_j},$$

where $\Delta V_j = \varepsilon_j A_j \Delta x_j$ is the nodal volume of acid in the j^{th} region, $\Delta c = |c^n - c_R^n|$ is the absolute change in acid concentration due to each reaction step, and K_j is the equivalent molar to charge ratio per region j.

To reduce our simulated voltage to match the worst charged battery of the batch, we

calibrate our maximum allowable nodal utilizations in the positive plate to 47%. In our experience, simulated voltages have always been positive-electrode limiting, because the positive electrode always seems to max out before the negative electrode. Thus, we only consider adjusting the positive utilization. From the standard 55%, this corresponds to a deficit of 8%, which would suggest that the shortest running battery was only 92% formed at the time of the initial discharge. Figure 19 provides a comparison between the calibrated simulated voltages to these two data strands on the extreme short and long end of the seven batteries tested.

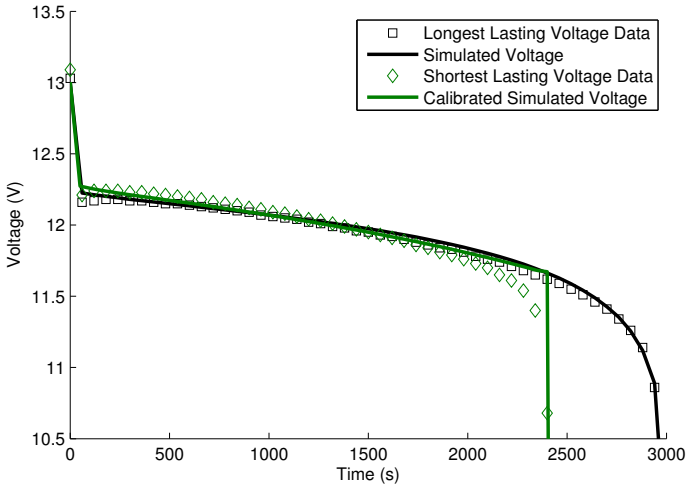

Figure 19: Comparison of simulated and measured battery voltages at 27 Amp discharge current for two data strands of various charge capacities representing the best and worst discharges of a particular test batch. The maximum allowable utilization is calibrated to simulate the variability.

3.6 Discussion

Our reduction to the simplified sulfuric acid model (3.2-3.10) produced results as expected. The operator splitting method used to separate this PDE into linear and solvable nonlinear pieces produced a smooth reaction-diffusion of the electrolyte. The profile of the acid concentration in Figure 13 smoothly decreases through reaction in the electrodes and diffusion from the separator into each electrode. The speed-up associated with using the operator splitting method in favor of a fully implicit solution is quite remarkable, especially for finer meshes (240 and 480 node discretizations). This computational speed-up is super-linear, as the acceleration in the speed-up factor stays above 1, and is in fact better than exponential speed-up as this acceleration also stays above one and is strictly increasing. Supported by these results, this decoupled operator splitting should be particularly effective for large scale systems.

A model for voltage was derived via the Nernst equation, (3.17), from this simulated concentration, and is used to compare with measured data. This data, however, is not uniform, as demonstrated in figure 18, though the batteries were manufactured to fit the same design. We developed a dependence on maximum allowable utilization to model this variability in the data. In calibrating our simulation to fit the data, we are able to determine the percentage of formation of each battery before they are cycled up to a more uniform charge formation. This percent formulation capacity relates the life of the battery to the conductivity of the formation of the battery electrodes.

Chapter 4

CONCLUDING REMARKS

With this dissertation, we explored numerical methods for solving semilinear parabolic PDEs using the idea of decoupled operator splitting. Further, we examined what stability considerations were needed, such as oscillation-free behavior, when extending methods past linear PDEs. We developed mathematical models from first principles and then reduced them down through simplifying assumptions. In verifying the models, we encountered real-life data that required model calibration and further model refinement.

Operator Splitting

Before a method is used to solve a problem, it must be analyzed to verify that it will give you a solution you can trust. Theorems 1.1 and 1.2 in section 1.1.4 were critical in proving that first and second order recombinations, as previously defined for linear problems, did indeed preserve first and second order accuracy, respectively, for semilinear parabolic PDEs. Further, the accuracy was verified in section 2.2.6 to demonstrate the theory to the second order and to show that the accuracy in time is affected by the splitting and is independent of the accuracy in space.

The reason we were drawn to operator splitting in the first place was the simplicity that it provided. Decoupled operator splitting allows for a separation of spatial dependence, as shown in all the applications, and further allows for access to exact solutions to some nonlinear, but separable, problems. We even explored nesting and combining various split recombination schemes to access further exact solutions and methods with higher order accuracy. Also, operator splitting simplified our stability analysis and the conditions required to have a stable and oscillation-free method.

One of the highlights of simplicity provided by operator splitting was computational

speed-up. The quick simulation run-time was hundreds, if not thousands, of times faster than real-time. Also, not only did the splitting allow for remarkable speed-up for fine meshes, but the acceleration factor of the speed-up showed that it was super-linear and in fact speeds up more than exponentially.

Oscillation-Free Conditions

It was a surprising observation that the standard, unconditionally stable Crank-Nicolson method allowed oscillatory behavior in linear PDEs (see figure 3) and that these oscillations led to actual instabilities in a nonlinear PDE (see figure 7). This demonstrated a weakness in our definition of stability and a warning to nonchalant use of numerical methods, which worked fine for linear problems, in solving nonlinear problems. As the positive eigenvalue condition for oscillation-free methods usually excludes a subset of the stable region, this oscillation-free condition should be used to define a stricter form of stability. Though helpful for linear PDEs, this stricter form of stability is required for solving some nonlinear PDEs in a stable fashion.

Modeling

We have explored the essence of mathematical modeling by developing models for acid concentration and battery voltage from first principles and then reducing them down through simplifying assumptions. This process of getting a feel for feasible parameter values and understanding the physical processes involved required interdisciplinary research and collaboration. Building up a model from basic theories provides an exercise in the deductive nature of science. Reducing a model down requires that we are tuned

in with the conditions of the experiment at hand. In sum, the modeling process has broadened the scope of the problem at hand and forced us to connect across fields to better understand the meaning of the mathematics.

Simulation

Once a model is developed, it is verified against certain data, like ours in figure 14, and then it is used to simulate and predict future behavior. To this end, we have calibrated parameters to make the model a better fit and to make it more versatile to known and unknown sources of variation in the data, and we look forward to utilizing it in the future to simulate further battery tests.

BIBLIOGRAPHY

[1] P. W. Appel, D. B. Edwards, and T. Stalick. Modeling the Effects of Electrolyte Diffusion and Paste Conductivity on Lead-Acid Battery Performance. *Journal of Power Sources*, 46:49–60, 1987.

[2] Philip W. Appel. *Modeling and Verifying the Performance of Lead-Acid Battery Cell with Paste Additives*. PhD thesis, University of Idaho, Moscow, ID USA, 1994.

[3] P.G. Balakrishnan and John Rethinam. *Electrochemical Studies of Batteries*. Nova Sciences Publishers, Inc, New York, 2005.

[4] Allen J. Bard and Larry R. Faulkner. *Electrochemical methods : fundamentals and applications*. Whiley, New York, 2nd edition, 1980.

[5] D. Berndt. *Mainenance-Free Batteries*. Research Studies Press, Ltd, Baldock, England, 3rd edition, 2003.

[6] Richard Burden and J. Douglas Faires. *Numerical Analysis*. PWS-Kent Pub Co, Boston, 5th edition, 1993.

[7] Rick Lee Cantrell. Modeling and Designing a High Performance Lead-Acid Battery for Hybrid Electrical Vehicle. Master's thesis, University of Idaho, Moscow, ID USA, 1996.

[8] J. Crank and P. Nicolson. A practical method for numerical evaluation of solutions of partial differential equations of the heat-conduction type. *Proc. Cambridge Philos. Soc.*, 43:50–67, 1947.

[9] T. R. Crompton. *Battery Reference Book*. Butterworth-Heinemann, Oxford, England, 2nd edition, 1995.

[10] M. Dehghan and A. Taleei. A compact split-step finite difference method for solving the nonlinear Schrödinger equations with constant and variable coefficients. *Computer Physics Communications*, 181:43–51, 2010.

[11] U. S. DOE. Weekly United States Spot Price F.O.B. Weighted by Estimated Import Volume. *Energy Information Administration*, 9/22/2010.

[12] U. S. DOE. Monthly u.s. total gasoline all sales/deliveries by prime supplier. *Energy Information Administration*, 9/23/2010.

[13] U. S. DOE. Weekly U.S. Petroleum Products Product Supplied. *Energy Information Administration*, 9/23/2010.

[14] J.S. Dunning. PhD thesis, University of California, Los Angeles, CA, 1971.

[15] J. Euler. Porendimensionen und oberflächenkapazität von braunstein. *Electrochimica Acta*, 4(1):27 – 41, 1961.

[16] R. A. Fisher. The wave of advance of advantageous genes. *Ann. Eugenics*, 7:353–369, 1937.

[17] Juergen Geiser. Operator Splitting Methods II: Classical and Iterative Operator-Splitting-methods. *Weierstrauss Institute for Applied Analysis and Stochastics*, 11th Lecture, 2006.

[18] Pritpal Singh Gill. A Finite Difference Model for Simulating the Discharge Behavior

of the Positive Electrode in Lead-Acid Cells. Master's thesis, University of Idaho, Moscow, ID USA, 1995.

[19] Hiram Gu, T.V. Nguyen, and R.E. White. A Mathematical Model of a Lead-Acid Cell. *Journal of Electrochemical Society*, 134(12), 1987.

[20] R. H. Hardin and F. D. Tapperta. Applications of the Split-Step Fourier Method to the Numerical Solution of Nonlinear and Variable Coefficient Wave Equations. *SIAM Rev. Chronicle*, 15:423, 1973.

[21] A. Kolmogorov. *Selected Works of A. N. Kolmogorov I: A study of the diffusion equation with increase in the amount of substance, and its application to a biological problem.* Kluwer, 2nd edition, 1991.

[22] J. C. Kotz and P. T. Treichel. *Chemistry and Chemical Reactivity.* Saunders College Publishers, Fort Worth, USA, 4th edition, 1999.

[23] I-Ming Lee and V. S. Manoranjan. Analysis of a Population Model with Efficient Resource Utilization. *Journal of Interdisciplinary Mathematics*, 13:41–50, 2010.

[24] H. Bauke M. Ruf and C. H. Keitel. A real space split operator method for the Klein-Gordon equation. *Journal of Computational Physics*, 228:9092–9106, 2009.

[25] V. S. Manoranjan. Numerical Studies of Reaction-Diffusion Problems. *University of Strathclyde seminars applied mathematical analysis: mathematics in medicine and biomechanics*, 7:73–90, 1984.

[26] G. I. Marchuk. *Handbook of Numerical Analysis: Finite Difference Methods (Part 1), Volume 1.* Elsevier, Amsterdam, 2003.

[27] P. L. Nash. A new fourth-order Fourier-Bessel split-step method for the extended nonlinear Schrödinger equation. *Journal of Computational Physics*, 227:2073–2082, 2008.

[28] J.D. Newell, S.N. Patankar, and D.B. Edwards. Porous Microspheres as Additives in Lead-Acid Batteries. *accepted for publication in: Journal of Power Sources*, 2010.

[29] J. Newman and W. H. Tiedemann. Porous-electrode theory with battery applications. *AIChE Journal*, 21:25, 1975.

[30] John Newman. Numerical solution of coupled, ordinary differential equations. *Industrial & Engineering Chemistry Fundamentals*, 7(3):514–517, 1968.

[31] J. Nocedal and S.J. Wright. *Numerical Optimization*. Spring-Verlag, New York, USA, 2nd edition, 2006.

[32] Anil Paryani. Concorde Battery Test For HE HMMWV. Technical report, Concorde Battery Corporation, West Covina, CA USA, 2007.

[33] Rubha Ponraj, Simon D. McAllister, I. Francis Cheng, and Dean B. Edwards. Investigation on Electrically Conductive Additives to Improve Positive Active Material Utilization in Lead-Acid Batteries. *Submitted for publication*, 2010.

[34] Werner Stein. Die vorgänge in den poren von masseplatten bei der entladung des bleisammlers mit großen stromdichten. *Naturwissenschaften*, 45:459–460, 1958.

[35] Gilbert Strang. On the Construction and Comparison of Difference Schemes. *SIAM Journal on Numerical Analysis*, 5, 1968.

[36] T. R. Taha and M. I. Ablowitz. Analytical and numerical aspects of certain nonlinear evolution equations. *II. Numerical, nonlinear Schrödinger equation*, 55:203, 1984.

[37] A. Tenno, R. Tenno, and T. Suntio. Charge-discharge behaviour of VRLA batteries. *Journal of Power Sources*, 103:42–53, 2001.

[38] J.A. Trainham. *Flow-through porous electrodes.* PhD thesis, University of California, Berkeley, CA, 1979.

[39] H. Q. Wang. Numerical studies on the split-step finite difference method for nonlinear Schrödinger equations. *Applied Mathematics and Computation*, 170:17–35, 2005.

[40] David S. Watkins. *Fundamentals of Matrix Computations.* John Wiley and Sons, 2nd edition, 2002.

[41] Wen-Chyuan Yueh. Eigenvalues of several tridiagonal matrice. *Applied Mathematics E-Notes*, 5:66–74, 2005.

[42] Song Zhang. *Investigating Paste Additives to Improve the Specific Energy Performance of a Lead Acid Battery.* PhD thesis, University of Idaho, Moscow, ID USA, 2005.

[43] V. Zharnitsky. Averaging for split-step scheme. *Nonlinearity*, 16:1359–1366, 2003.